Powder Technology 367 (2020) 192–205

Contents lists available at ScienceDirect

Powder Technology

journal homepage: www.elsevier.com/locate/powtec

MHD flow and heat transfer near stagnation point over a stretching/shrinking surface with partial slip and viscous dissipation: Hybrid nanofluid versus nanofluid

Emad H. Aly [a,*], I. Pop [b]

[a] Department of Mathematics, Faculty of Science, University of Jeddah, Jeddah, Saudi Arabia
[b] Department of Mathematics, Babeş-Bolyai University, 400084 Cluj-Napoca, Romania

ARTICLE INFO

Article history:
Received 30 November 2019
Received in revised form 14 February 2020
Accepted 10 March 2020
Available online 16 March 2020

Keywords:
MHD flow
Heat transfer
Hybrid nanofluid
Stretching/shrinking sheet
Dual solution
Stability analysis

ABSTRACT

The steady magnetohydrodynamic stagnation point flow and heat transfer over a stretching/shrinking surface in a hybrid nanofluid with partial slip and viscous dissipation were theoretically/numerically studied. The governing equations of the problem were turned into ODEs by using appropriate transformations. The plots of most important parameters were presented for both surfaces. It was found that on increasing the magnetic parameter, the hybrid nanofluid is better as a heater rather than nanofluid, however, it is better as a cooler on rising Eckert number, the stretching and slip parameters. For shrinking sheet, critical regions of unique/dual solution have been introduced. Further, stability of the unique/dual solution was studied where three regions of stability were noticed. It was deduced that the velocity and temperature are sensitively available close to the terminated line in the dual solution region. It was also proved that their behavior is absolutely different over the three regions of stability.

© 2020 Elsevier B.V. All rights reserved.

1. Introduction

Heat transfer enhancement is a very important problem in engineering and industrial applications nowadays. Cooling liquid such as water, ethylene glycol and oil which have low thermal conductivity are used as pure fluids in many applications, thus limiting the heat transfer enhancement. However, new types of fluids called nanofluids were introduced by Choi [1] in 1995 in order to get improvement in thermal efficiency. He expected that the addition of metallic nanoparticles in the base fluids can essentially improve the thermal conductivity of the conventional base fluids and enhance the heat transfer execution of these fluids. Nanofluids are used as coolants, lubricants, and also in practical applications including refrigeration and air–conditioning, microelectronics, computers' processors, etc. In recent years, the behavior and characteristics of nanofluids in different problems have been studied experimentally and numerically by many researchers. For example, Hwang et al. [2] estimated thermal conductivity of different nanofluids and demonstrated that the thermal conductivity improvement of nanofluids relied upon the volume fraction of the suspended particles and the thermal conductivities of the particles and base fluids. Wang and Su [3] performed an experimental investigation of nanofluid flow and heat transfer in a vertical tube under different pressure conditions. Ahmadi and Willing [4] studied experimentally the heat transfer measurement in water based nanofluids and developed model of computational fluid dynamics (CFD) using Eulerian–Lagrangian approach to study the nature of both the laminar and turbulent flow fields of the fluid and the dispersed nanoparticles.

In addition, the investigation on the mathematical models of nanofluid is reported by many researchers. There are two common types of nanofluid models that have been considered in fluid dynamics, namely the model proposed by Buongiorno [5] and Tiwari and Das [6]. Some researchers such as Kuznetsov and Nield [7], Rohni et al. [8], and Bachok et al. [9] used the mathematical nanofluid model proposed by Buongiorno [5], which takes into account the effects of Brownian motion and thermophoresis parameters. The nanofluid model proposed by Tiwari and Das [6] was also employed by several authors such as Rohni et al. [10]. Comprehensive reviews on synthesis, stability, thermophysical properties, characterization, applications and potential future directions of nanofluids have been recently introduced by Chamkha et al. [11], Nadooshan et al. [12] and Sezer et al. [13].

To find a better type of fluid instead of nanofluid, a unique type of nanofluids called 'hybrid nanofluids' are introduced. Hybrid nanofluid is an extension of nanofluid which is composed of two different nanoparticles dispersed in the base fluid. This kind of fluid is believed to offer good thermal characteristics when compared with the base fluid and nanofluid containing single nanoparticles. Hybrid nanofluids are widely applied in many heat transfer fields such as electronic cooling,

* Corresponding author.
E-mail addresses: efarag@uj.edu.sa (E.H. Aly), ipop@math.ubbcluj.ro (I. Pop).

https://doi.org/10.1016/j.powtec.2020.03.030
0032-5910/© 2020 Elsevier B.V. All rights reserved.

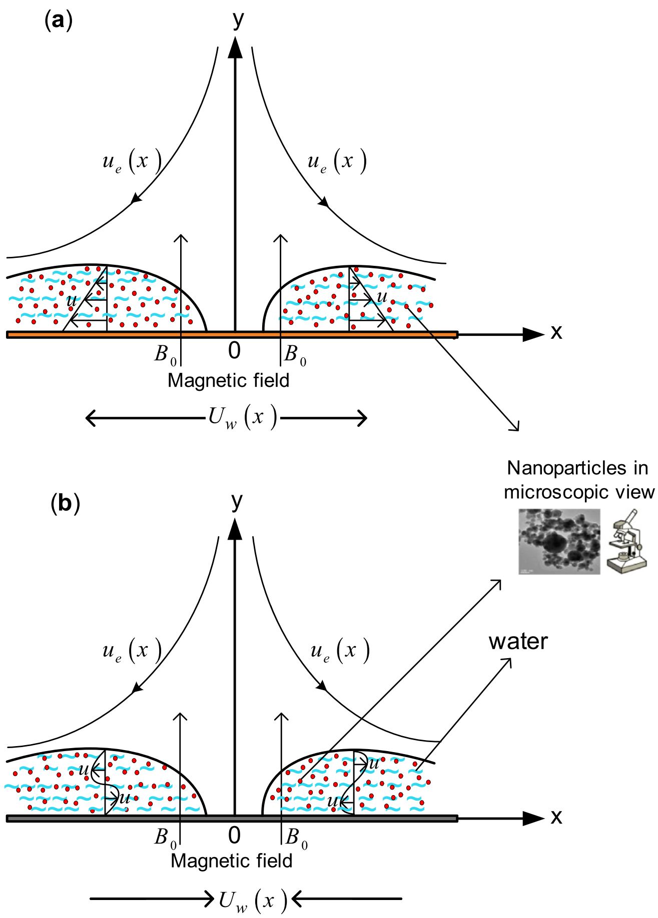

Fig. 1. Physical model and coordinate system for (a) Stretching sheet and (b) Shrinking sheet.

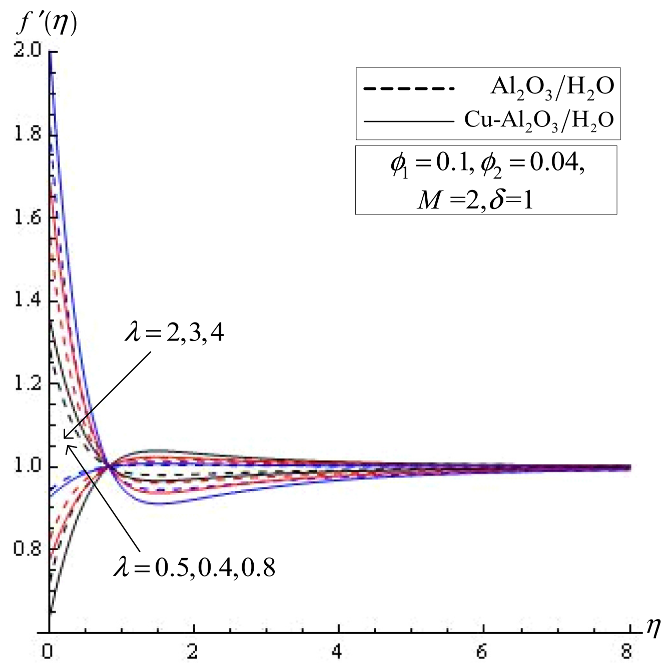

Fig. 2. Velocity profiles of Al_2O_3/H_2O vt. $Cu–Al_2O_3/H_2O$ for various values of $\lambda < 1$ and $\lambda > 1$ (stretching sheet).

generator cooling, coolant in machining, nuclear system cooling, transformer cooling, biomedical, drug reduction and refrigeration with better efficiency compared to nanofluids applicability.

The capability of hybrid nanofluids in enhancing the thermal characteristics attracts the researchers to study them in the real world heat transfer problems ([14,15]). For example, the effect of Al_2O_3-Cu/water hybrid nanofluid in heat transfer was reported by Suresh et al. [16]. Synthesis of spherical silica/multiwall carbon nanotubes hybrid nanostructures of related nanofluids was analyzed by Baghbanzadeha et al. [17]. Later, Vafaei et al. [18] predicted the thermal conductivity of MgO-MWCNTs/EG hybrid nanofluid at volume fractions of 0.05–0.6% and temperature 25–50 °C using several experimental methods.

Furthermore, the influence of nanofluid with double nanoparticles in a flat plate solar collector using finite element simulation was examined by Nasrin and Alim [19]. Takabi and Shokouhmand [20] conveyed the effects of Al_2O_3-Cu/water hybrid nanofluid on heat transfer and flow characteristics in turbulent regime. Devi and Devi [21] investigated the problem of three–dimensional hybrid $Cu–Al_2O_3$/water nanofluid flow over a stretching sheet with effecting Lorentz force subject to Newtonian heating. Later, Devi and Devi [22] studied the heat transfer enhancement of $Cu–Al_2O_3$/water hybrid nanofluid flow over a stretching sheet. Stagnation–point flow of an aqueous titania–copper hybrid nanofluid toward a wavy cylinder was investigated by Yousefi et al. [23]. Rotating flow of $Ag–CuO/H_2O$ hybrid nanofluid with radiation and partial slip boundary effects was studied by Hayat et al. [24]. Recently, there is more numerical investigation involving hybrid nanofluids with different cases, see for example Ghadikolaei et al. [25], Tayebi and Chamkha [26] and Ghalambaz et al. [27].

Table 1
Thermophysical properties of the water and nanoparticles [56].

Physical properties	Base fluid	Nanoparticles	
	Water	Al_2O_3	Cu
ρ (kg m^{-3})	997.1	3970	8933
C_p (J kg^{-1} K^{-1})	4179	765	385
k (W m^{-1} K^{-1})	0.613	40	401
σ (Ω^{-1} m^{-1})	0.05	1×10^{-10}	5.96×10^7

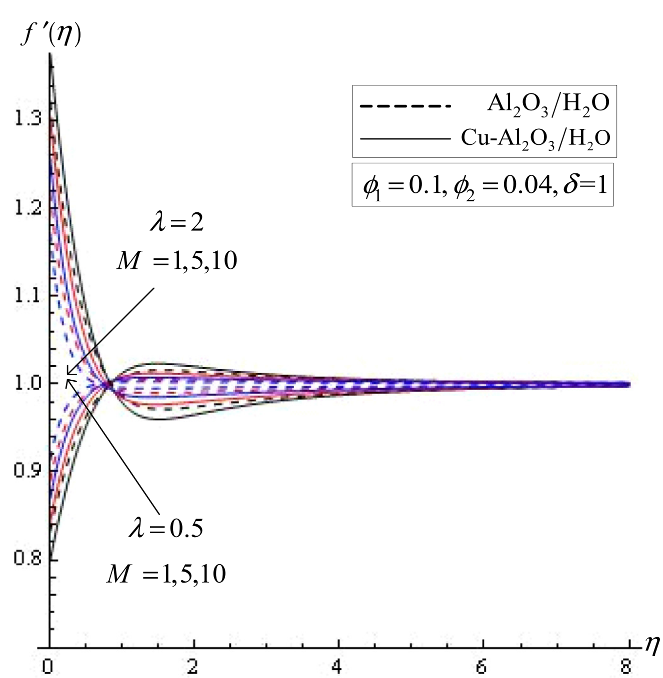

Fig. 3. Velocity profiles of Al_2O_3/H_2O vt. $Cu–Al_2O_3/H_2O$ for various values of M when $\lambda = 0.5$ and 2 (stretching sheet).

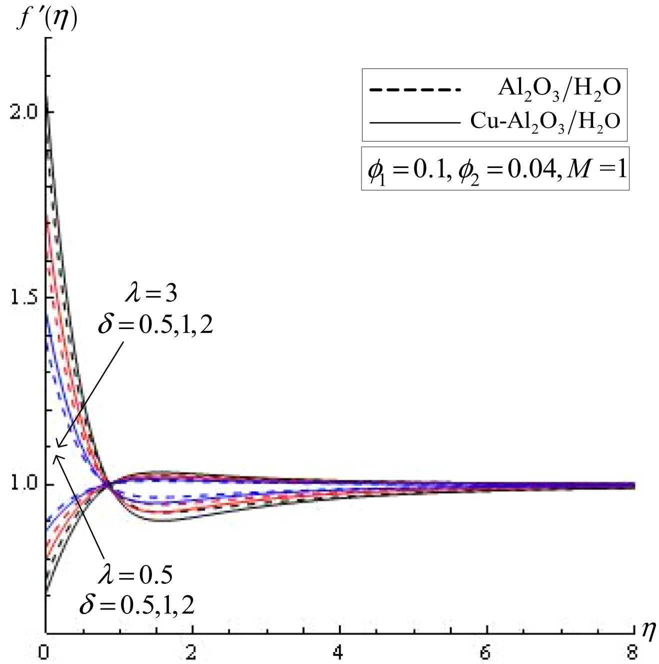

Fig. 4. Velocity profiles of Al_2O_3/H_2O vt. $Cu–Al_2O_3/H_2O$ for various values of δ when $\lambda = 0.5$ and 3 (stretching sheet).

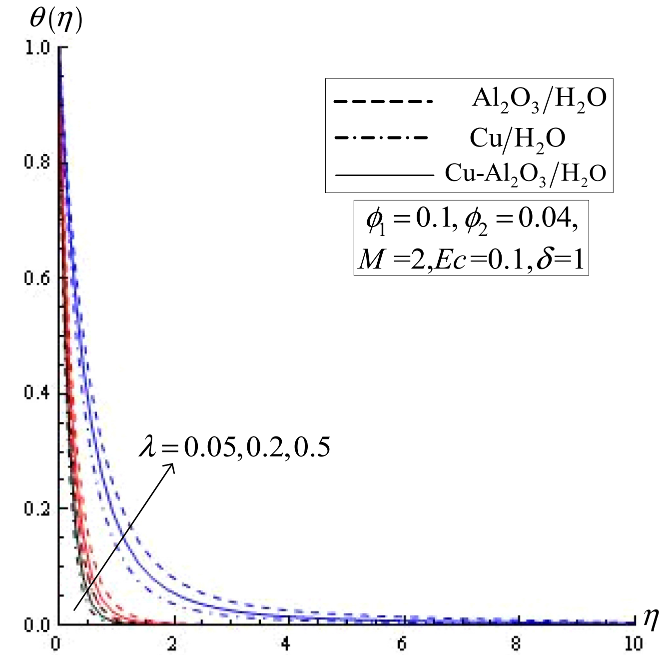

Fig. 6. Temperature distributions of Al_2O_3/H_2O and Cu/H_2O vt. $Cu–Al_2O_3/H_2O$ for various values of λ.

There are many parameters that highly contribute to the heat transfer enhancement of hybrid nanofluid such as base fluid selection, nanoparticles size, viscosity, fluid temperature and stability, dispersibility of the nanoparticles, purity of nanoparticles, preparation method, size and shape of nanoparticles and compatibility of the nanoparticles that lead to harmonious mixture of the nanofluid. For instance, the collection of papers on nanofluids or hybrid nanofluids can be found in the books by Minkowycz et al. [28] and Shenoy et al. [29] and in the review papers by Buongiorno et al. [30], Bahiraei et al. [31], Sezer et al. [13], Mahian et al. ([32,33]), Sarkarn et al. [34], Babu et al. [35], Huminic and Huminic [36], Sidik et al. [37], Sundar et al. [38] and Asadi et al. [39]. Recently, Aparna et al. [40] have experimentally investigated the thermal conductivity of aqueous Al_2O_3/Ag hybrid nanofluid at different temperatures and volume concentration. Very recently, experimental study on stability and rheological behavior of hybrid Al_2O_3-TiO_2 Therminol-55 nanofluids for concentrating solar collectors has been studied by Gulzar et al. [41].

The fluid dynamics due to a stretching sheet has important applications in industries such as the hot rolling, wire drawing and glass–fiber production. In view of these applications, Sakiadis [42] first investigated

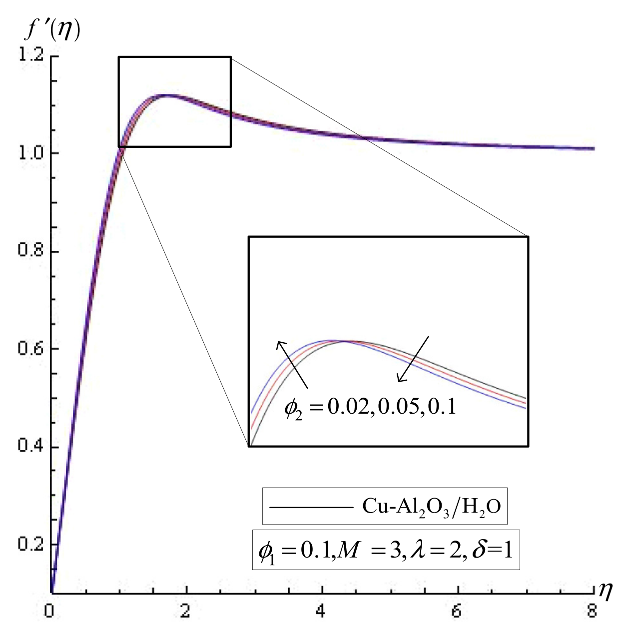

Fig. 5. Effect of ϕ_2 on the velocity profiles of $Cu–Al_2O_3/H_2O$ over a stretching sheet.

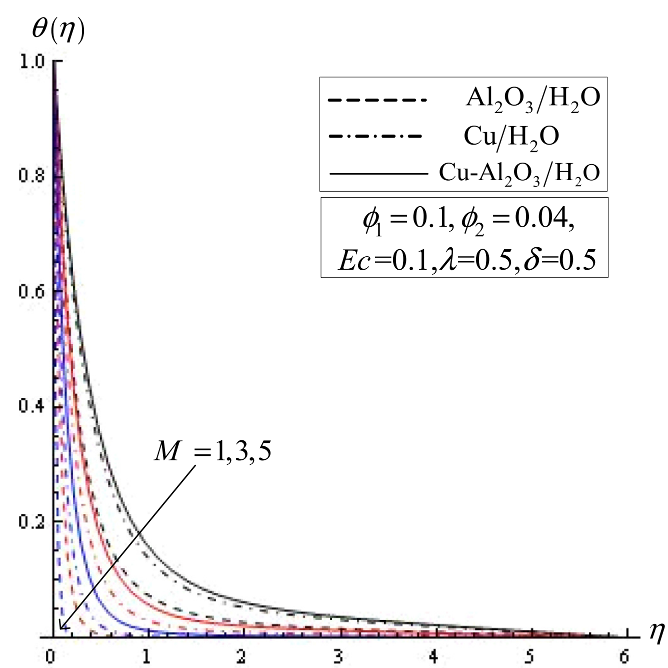

Fig. 7. Effects of M on temperature distributions for Al_2O_3/H_2O and Cu/H_2O vt. $Cu–Al_2O_3/H_2O$.

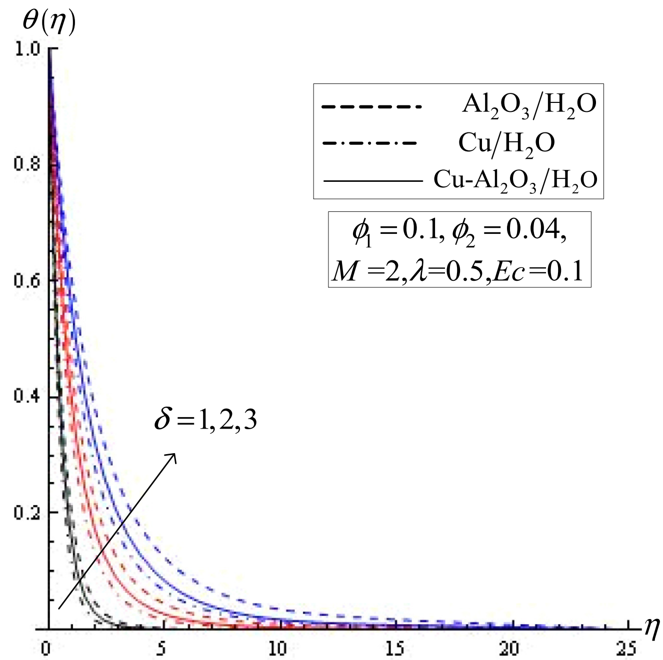

Fig. 8. Varying of δ on temperature distributions for Al_2O_3/H_2O and Cu/H_2O vt. $Cu–Al_2O_3/H_2O$.

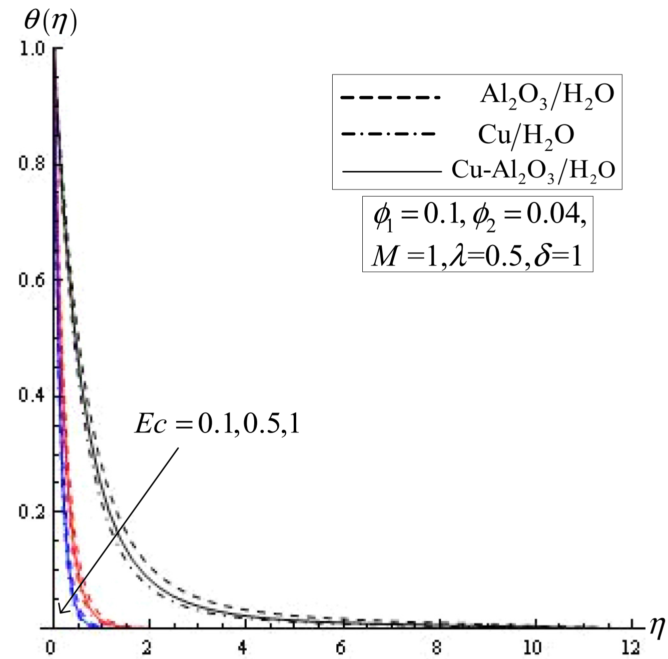

Fig. 10. Temperature distributions of Al_2O_3/H_2O and Cu/H_2O vt. $Cu–Al_2O_3/H_2O$ for various values of *Ec*.

the boundary layer flow on a continuous solid surface moving at constant speed. Since the pioneering study by Crane [43], who presented an exact analytical solution for the steady two–dimensional flow due to a stretching surface in a quiescent fluid, many authors have considered various aspects of this problem and obtained similarity solutions such as Magyari [44] and Ishak et al. [45]. However, instead of considering the case of stretching sheet, researchers also investigated the case of shrinking sheet. This new type of shrinking sheet flow is essentially a backward flow as discussed by Goldstein [46]. The development of this unusual type of flow due to shrinking was first observed by Wang [47] when he investigated the behavior of a liquid film on an unsteady stretching sheet. Miklavčič and Wang [48] investigated the steady flow over a shrinking sheet, which is an exact solution of the Navier–Stokes equations. They found that mass suction is required to maintain the flow over a shrinking sheet. The flow induced by a shrinking sheet with constant velocity or power–law velocity distribution was investigated by Fang and Zhang [49]. The shrinking sheet problem was also extended to other fluids and various geometries with different conditions by many researchers such as Merkin and Kumaran [50], Soid et al. [51] and Pop et al. [52], Waini et al. [53] and Khashi'ie et al. [54]. Further, Rohni et al. [10] solved the problem of shrinking sheet immersed in nanofluids for three types of nanoparticles which are copper, alumina and titania by considering water as the based fluid.

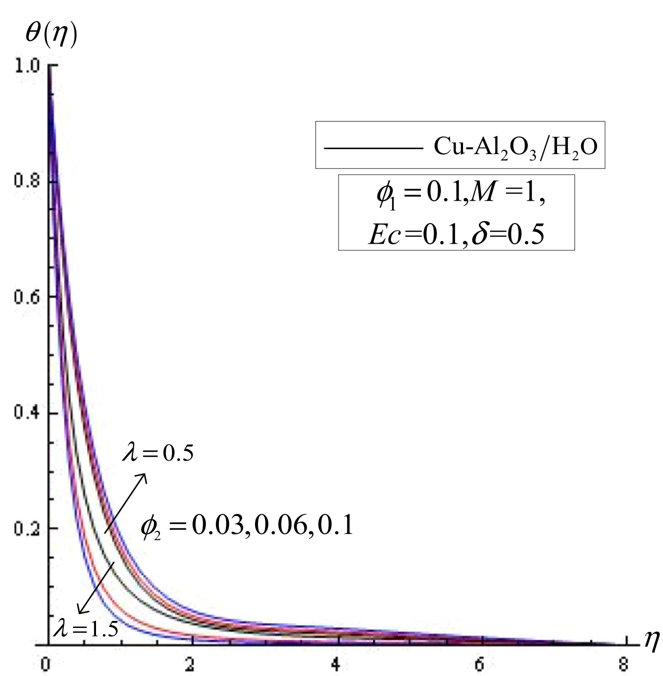

Fig. 9. Temperature distributions of $Cu–Al_2O_3/H_2O$ for various values of ϕ_2 when $\lambda = 0.5$ and 1.5.

Motivated by the above studies, the present paper aims to investigate the problem of the steady MHD flow and heat transfer of a hybrid nanofluid past a stretching/shrinking sheet with wall mass suction by employing nanofluid equations model proposed by Tiwari and Das [6]. Hybrid nanofluid is considered by suspending two different nanoparticles which are Al_2O_3 and then Cu in a pure water. Upon using the similarity transformations, the governing equations with boundary conditions are to be transformed into a system of ordinary differential equations. The system of equations is then solved exactly for the stream function and numerically for the temperature distributions. Therefore, the effects of several parameters on the flow and heat transfer characteristics are to be presented in graphical form.

2. Mathematical model

Consider a steady two–dimensional magnetohydrodynamic (MHD) boundary layer flow and heat transfer of a hybrid nanofluid over a permeable flat plate, where x and y axes are the Cartesian coordinates. In particular, the x axis and y axis are measured along the plate and normal to it, respectively, where the plate is located at $y = 0$, see Fig. 1. It is assumed that the surface is stretched/shrinked with the velocity $U_w(x)$, the velocity of the ambient (inviscid) fluid is $u_e(x)$ and the temperature of the surface is $T_w(x)$, while the constant temperature of the ambient hybrid nanofluid is T_∞. Further, the viscous dissipation effect and Joule

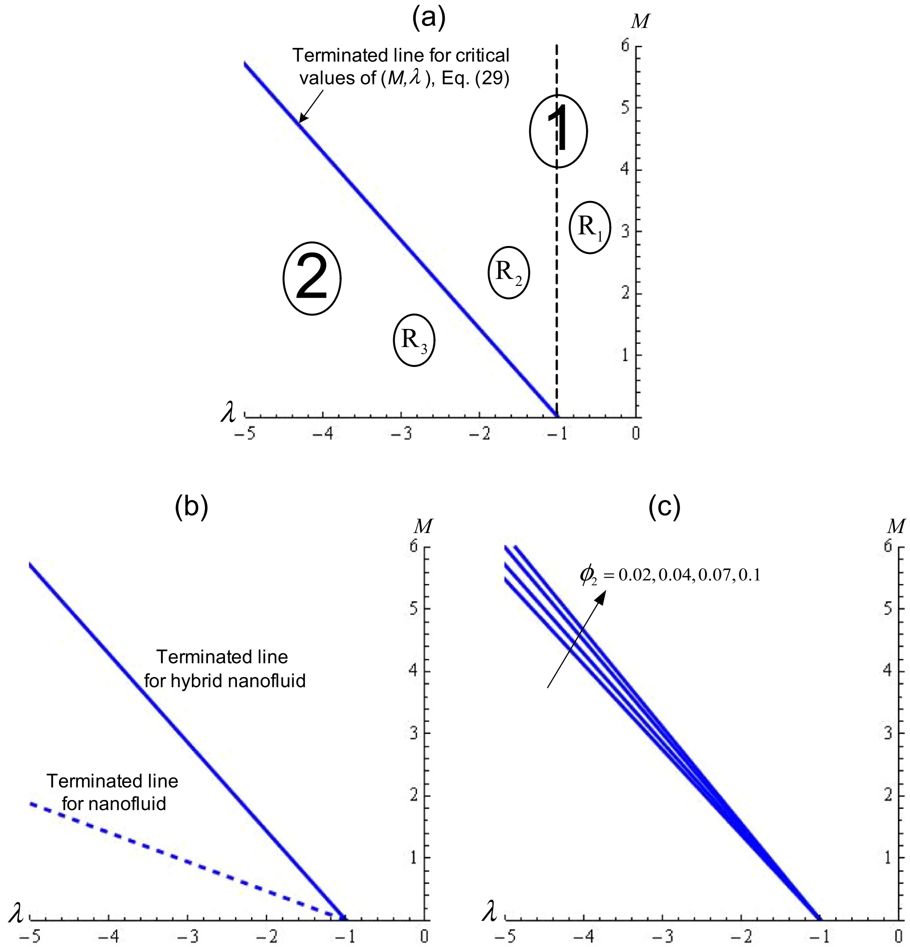

Fig. 11. Regions of unique and dual solutions of M as a function of $\lambda < 0$ (shrinking sheet) when $\delta = 1$ and $\phi_1 = 0.1$ for (a) hybrid nanofluid where $\phi_2 = 0.04$ (R_i, $i = 1,2,3$ call regions one, two and three, respectively), (b) terminated line of hybrid nanofluid ($\phi_2 = 0.04$) versus nanofluid ($\phi_2 = 0$) and (c) various values of ϕ_2.

heating are taken into consideration. Furthermore, a uniform transverse magnetic field of strength B_0 is applied parallel to the y-axis. It is also assumed that the hybrid nanofluid is electrically conductive and the magnetic Reynolds number is small so that the induced magnetic field is neglected. On investigating the hybrid nanofluid, it is assumed that the size of nanoparticles is uniform, and the effect of the agglomeration of nanoparticles on the thermophysical properties is neglected. Therefore, on employing the usual boundary layer approximation, the governing equations of the hybrid nanofluids are written as (Pop et al. [55], Yousefi et al. [23]):

$$\frac{\partial u}{\partial x} + \frac{\partial v}{\partial y} = 0, \tag{1}$$

Table 2
Values of the unique and dual solutions for various values of λ (shrinking sheet) vt. M for the hybrid nanofluid Cu–Al_2O_3/H_2O with $\phi_1 = 0.1$ and $\phi_2 = 0.04$, where $M_{c_1} = 1.4263$ and $M_{c_2} = 2.8526$, see Fig. 11.

λ	M	C_2	C_3	λ	M	C_2	C_3
−2	0.1	1.69211	0.335911	−3	0.5	1.60778	0.581027
	0.4	1.81291	0.239704		1	1.83573	0.393466
	0.7	1.91937	0.158295		1.5	2.01332	0.257172
	1	2.01575	0.087397		2	2.16456	0.148034
	1.2	2.07567	0.044689		2.5	2.29884	0.056596
	M_{c_1}	2.14005	0		M_{c_2}	2.38604	0
	2	2.29028			3	2.42099	
	2	2.52012			4	2.63945	
	5	2.90495			5	2.83341	

$$u\frac{\partial u}{\partial x} + v\frac{\partial u}{\partial y} = u_e\frac{du_e}{dx} + \frac{\mu_{hnf}}{\rho_{hnf}}\frac{\partial^2 u}{\partial y^2} + \frac{\sigma_{hnf}B_0^2}{\rho_{hnf}}(u_e - u), \tag{2}$$

$$u\frac{\partial T}{\partial x} + v\frac{\partial T}{\partial y} = \frac{1}{(\rho C_p)_{hnf}}\left[k_{hnf}\frac{\partial^2 T}{\partial y^2} + \mu_{hnf}\left(\frac{\partial u}{\partial y}\right)^2 + \sigma_{hnf}B_0^2\,(u_e - u)^2\right], \tag{3}$$

subject to the boundary conditions

$$v = 0, \quad u = U_w(x)\lambda + b\frac{\mu_{hnf}}{\rho_{hnf}}\frac{\partial u}{\partial y}, \quad T = T_w(x) \ \text{ at } \ y = 0, \tag{4a}$$

$$u \to u_e(x), \qquad T \to T_\infty \ \text{ as } \ y \to \infty. \tag{4b}$$

Here u and v are the velocity components of the hybrid nanofluid along x- and y-axes, $b > 0$ is the molecular mean free path (see Fang et al. [58]). Further, μ_{hnf} is the dynamic viscosity of the hybrid nanofluids, ρ_{nhf} is the density of the hybrid nanofluids, k_{hnf} is the thermal conductivity of the hybrid nanofluid, $(\rho C_p)_{hnf}$ is the heat capacity of the hybrid nanofluid, σ_{hnf} is the electrical conductivity of the hybrid nanofluids. Furthermore, $U_w(x) = u_e(x) = ax$, where a and T_0 are positive constants and L is the characteristic length of the stretching/shrinking surface. Moreover, $(\ )_{hnf}$ denotes the hybrid nanofluid quantities which are defined as follows (see Devi and Devi [21] and Gorla et al. [59])

$$\frac{\rho_{hnf}}{\rho_f} = (1 - \phi_2)\left[1 - \phi_1 + \phi_1\frac{\rho_{s_1}}{\rho_f}\right] + \phi_2\frac{\rho_{s_2}}{\rho_f}, \tag{5a}$$

$$\frac{\mu_{hnf}}{\mu_f} = \frac{1}{(1-\phi_1)^{2.5}(1-\phi_2)^{2.5}}, \tag{5b}$$

$$\frac{\sigma_{hnf}}{\sigma_f} = \frac{\sigma_{s_2}+2\sigma_{bf}+2\phi_2(\sigma_{s_2}-\sigma_f)}{\sigma_{s_2}+2\sigma_{bf}-\phi_2(\sigma_{s_2}-\sigma_f)}, \text{ where } \frac{\sigma_{bf}}{\sigma_f} = \frac{\sigma_{s_1}+2\sigma_f+2\phi_1(\sigma_{s_1}-\sigma_f)}{\sigma_{s_1}+2\sigma_f-\phi_1(\sigma_{s_1}-\sigma_f)}, \tag{5c}$$

$$\frac{k_{hnf}}{k_f} = \frac{k_{s_2}+2k_{bf}+2\phi_2(k_{s_2}-k_f)}{k_{s_2}+2k_{bf}-\phi_2(k_{s_2}-k_f)}, \text{ where } \frac{k_{bf}}{k_f} = \frac{k_{s_1}+2k_f+2\phi_1(k_{s_1}-k_f)}{k_{s_1}+2k_f-\phi_1(k_{s_1}-k_f)}, \tag{5d}$$

$$\frac{(\rho C_p)_{hnf}}{(\rho C_p)_f} = (1-\phi_2)\left[1-\phi_1+\phi_1\frac{(\rho C_p)_{s_1}}{(\rho C_p)_f}\right]+\phi_2\frac{(\rho C_p)_{s_2}}{(\rho C_p)_f}, \tag{5e}$$

where ϕ_1 and ϕ_2 are the hybrid nanoparticle volume fractions ($\phi_1 = \phi_2 = 0$ correspond to a regular fluid), ρ_f is the density of the base fluid,

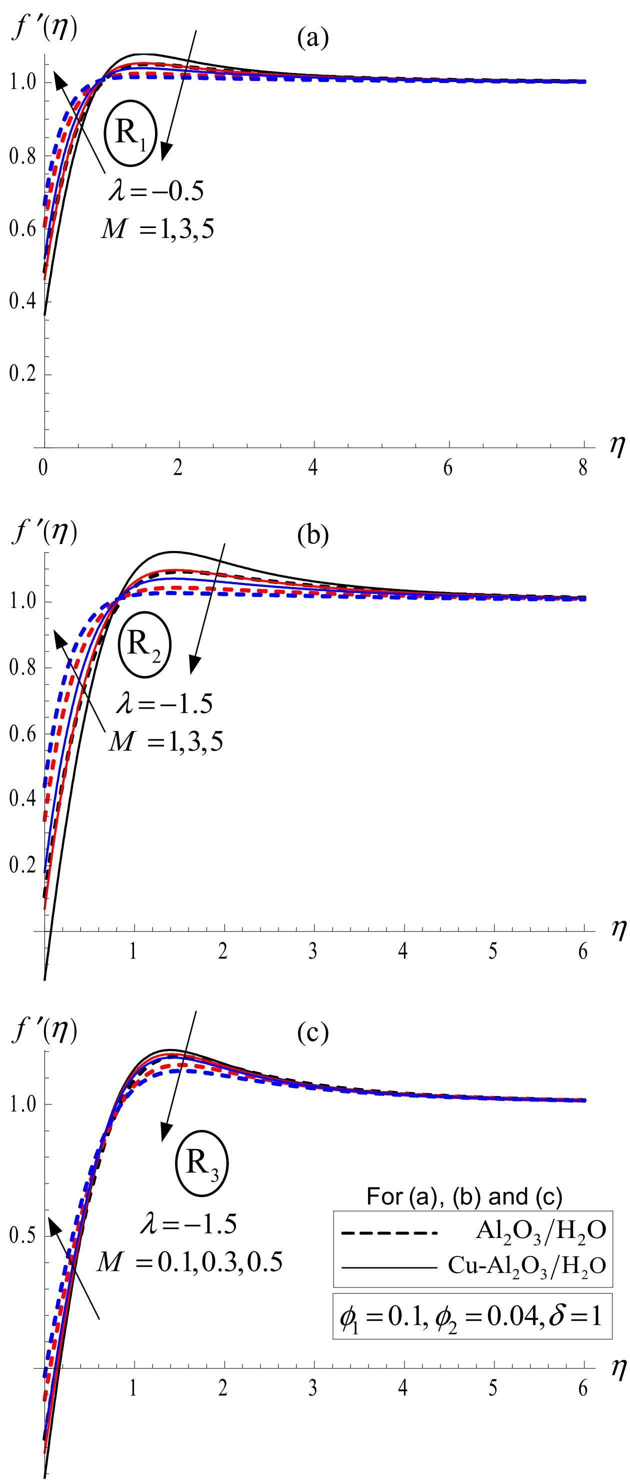

Fig. 12. Velocity profiles of the first solution; Al_2O_3/H_2O vt. Cu–Al_2O_3/H_2O for various values of M on the three regions of λ < 0 (shrinking sheet).

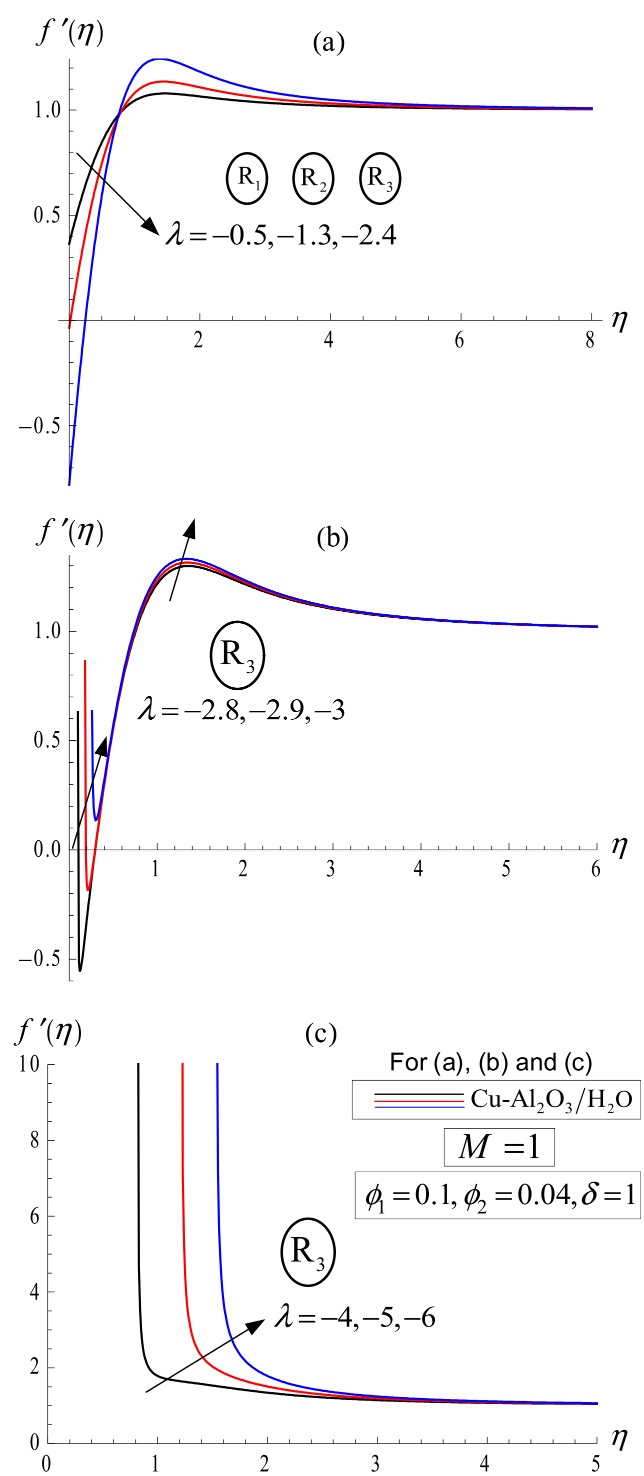

Fig. 13. Velocity profiles of the first solution for Cu–Al_2O_3/H_2O at various values of λ < 0 (shrinking sheet) and different regions.

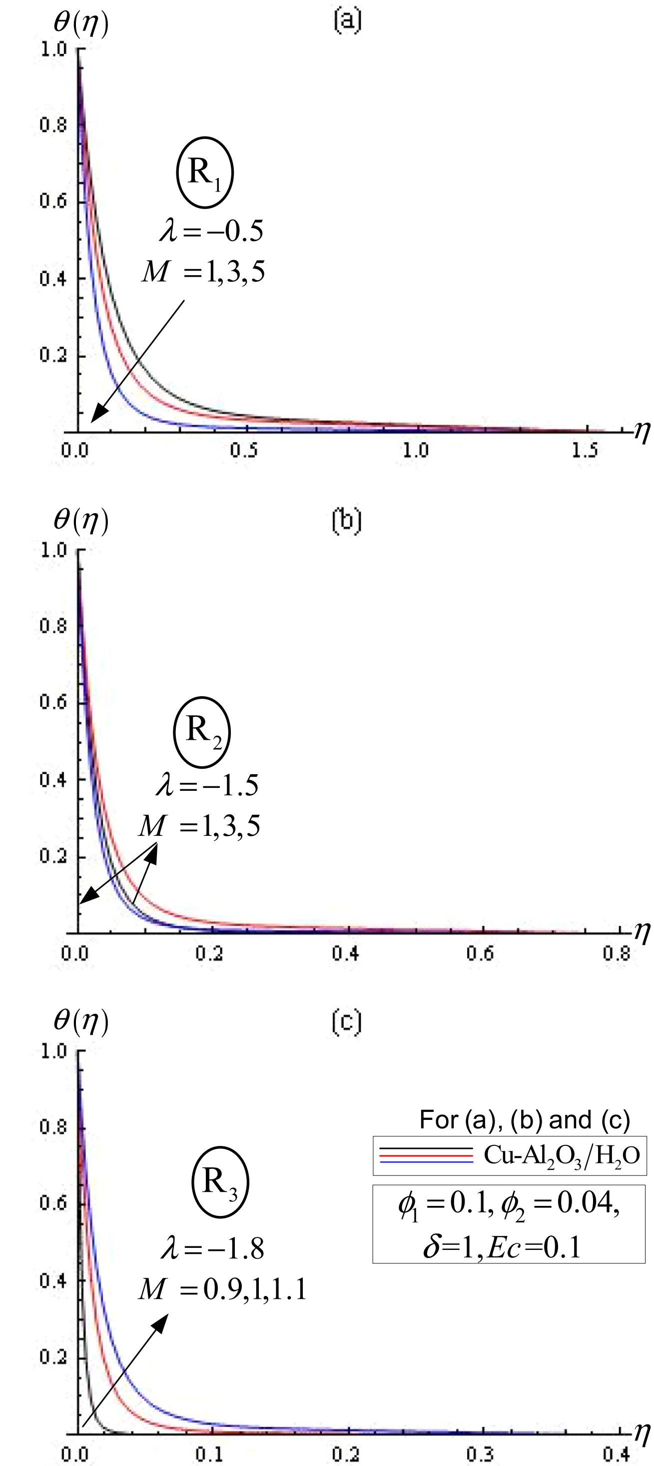

Fig. 14. Temperature distributions of the first solution for Cu–Al_2O_3/H_2O at various values of M on the three regions of $\lambda < 0$ (shrinking sheet).

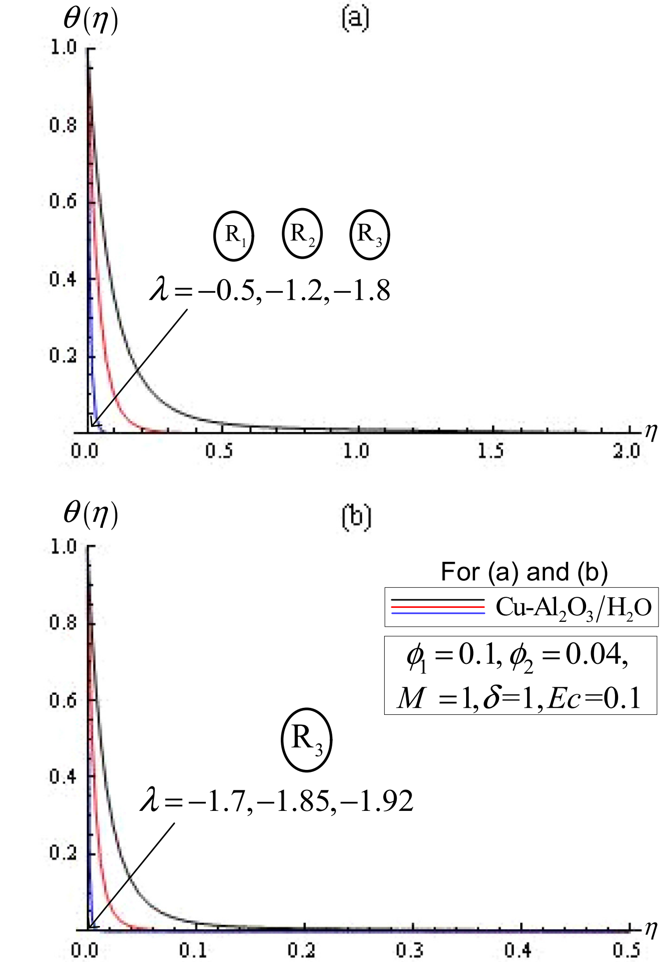

Fig. 15. Temperature distributions of the first solution for Cu–Al_2O_3/H_2O at various values of $\lambda < 0$ (shrinking sheet) and different regions.

ρ_{s_1} and ρ_{s_2} are the densities of the hybrid nanoparticles, k_f is the thermal conductivity of the base fluid, k_{s_1} and k_{s_2} are the thermal conductivities of the hybrid nanoparticles, $(\rho C_p)_f$ is the heat capacity of the base fluid. $(\rho C_p)_{s_1}$ and $(\rho C_p)_{s_2}$ are the heat capacitance of the hybrid nanoparticles, σ_f is the electrical conductivity of the base fluid, σ_{s_1} and σ_{s_2} are the electrical conductivities of the hybrid nanoparticles, and C_p is the heat capacity at the constant pressure of the base fluid. Moreover, the physical properties of the investigated base fluid (water), alumina (Al_2O_3) and copper (Cu) hybrid nanofluids are given in Table 1. Now, on using the following similarity variables

$$u = U_w(x) f'(\eta), \quad v(x,y) = -\sqrt{a\nu_f} f(\eta), \quad \theta(\eta) = \frac{T - T_\infty}{T_f - T_\infty}, \quad \eta = y\sqrt{\frac{a}{\nu_f}}, \tag{6}$$

Eqs. (2) and (3) along with the boundary conditions (4) are transformed into the following ordinary (similarity) differential equations

$$\alpha_2 f''' + \alpha_1 \left(f f'' - f'^2 + 1 \right) + \alpha_3 M (1 - f') = 0, \tag{7}$$

$$\frac{\alpha_5}{\alpha_4 \, Pr} \theta'' + f\theta' - 2f'\theta + Ec \left[\frac{\alpha_2}{\alpha_1} f''^2 + \alpha_3 (f' - 1)^2 \right] = 0, \tag{8}$$

subject to the boundary conditions (see Hayat et al. [24])

$$f(0) = 0, \quad f'(0) = \lambda + \delta \frac{\alpha_2}{\alpha_1} f''(0), \quad \theta(0) = 1, \tag{9a}$$

$$f'(\eta) \to 1, \quad \theta(\eta) \to 0 \quad \text{as} \quad \eta \to \infty, \tag{9b}$$

where α_i, $i = 1$ to 5, are defined as

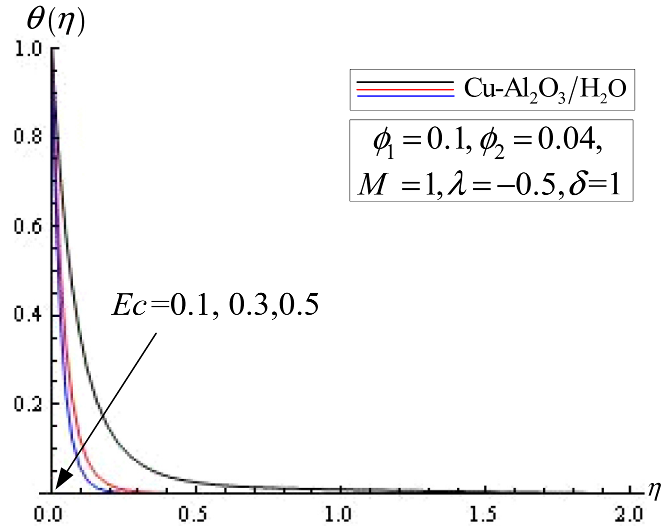

Fig. 16. Influence of the Eckert number on the temperature distribution for Cu–Al$_2$O$_3$/H$_2$O when $\lambda = -0.5$, i.e. shrinking sheet.

$$\alpha_1 = \frac{\rho_{hnf}}{\rho_f}, \quad \alpha_2 = \frac{\mu_{hnf}}{\mu_f}, \quad \alpha_3 = \frac{\sigma_{hnf}}{\sigma_f}, \quad \alpha_4 = \frac{(\rho C_p)_{hnf}}{(\rho C_p)_f} \quad \text{and} \quad \alpha_5 = \frac{k_{hnf}}{k_f}. \tag{10}$$

Here primes denote differentiation with respect to η, $Pr\left[=\frac{\nu_f}{\alpha_f}\right]$ is Prandtl number, $M\left[=\frac{\sigma_f B_0^2}{a\rho_f}\right]$ is the constant magnetic parameter, $\delta\left[=b\sqrt{a\nu_f}(>0)\right]$ is the velocity slip parameter and $Ec\left[=\frac{U_w^2(x)}{c_p(T_w-T_\infty)}=\frac{aL^2}{C_pT_0}\right]$ is Eckert number, which is a measure of the viscous dissipation. It is worth mentioning that when $\phi_1=\phi_2=M=0$ and $\lambda=1$ (stretching sheet), Eq. (7) deduces to Eq. (12) in Mahapatra and Gupta [57].

The physical quantities of interest are the skin friction coefficient C_f and the local Nusselt number Nu_x, which are defined as

$$C_f = \frac{\tau_w}{\rho_f U_w^2}, \qquad Nu_x = \frac{xq_w}{k_f(T_w-T_\infty)}, \tag{11}$$

where τ_w is the skin friction or shear stress along the plate and q_w is the heat flux from the plate, which are given by

$$\tau_w = -\mu_{hnf}\left(\frac{\partial u}{\partial y}\right)_{y=0}, \quad q_w = -k_{hnf}\left(\frac{\partial T}{\partial y}\right)_{y=0}. \tag{12}$$

On using Eqs. (6) and (12), we get

$$\mathrm{Sr} = C_f\sqrt{Re_x} = -\alpha_2 f''(0), \qquad \mathrm{Nur} = \frac{Nu}{\sqrt{Re_x}} = -\alpha_5\,\theta'(0), \tag{13}$$

where $Re_x = \frac{U_w(x)x}{\nu_f}$ is the local Reynolds number.

3. Analytical solution for the fluid flow

The solution $f(\eta)$ in Eq. (7), which fulfills the boundary conditions (9), can be deduced as

$$f(\eta) = \eta + \frac{\alpha_1(\lambda-1)}{\delta\alpha_2 C^2 + \alpha_1 C}\left(1-e^{-C\eta}\right), \tag{14}$$

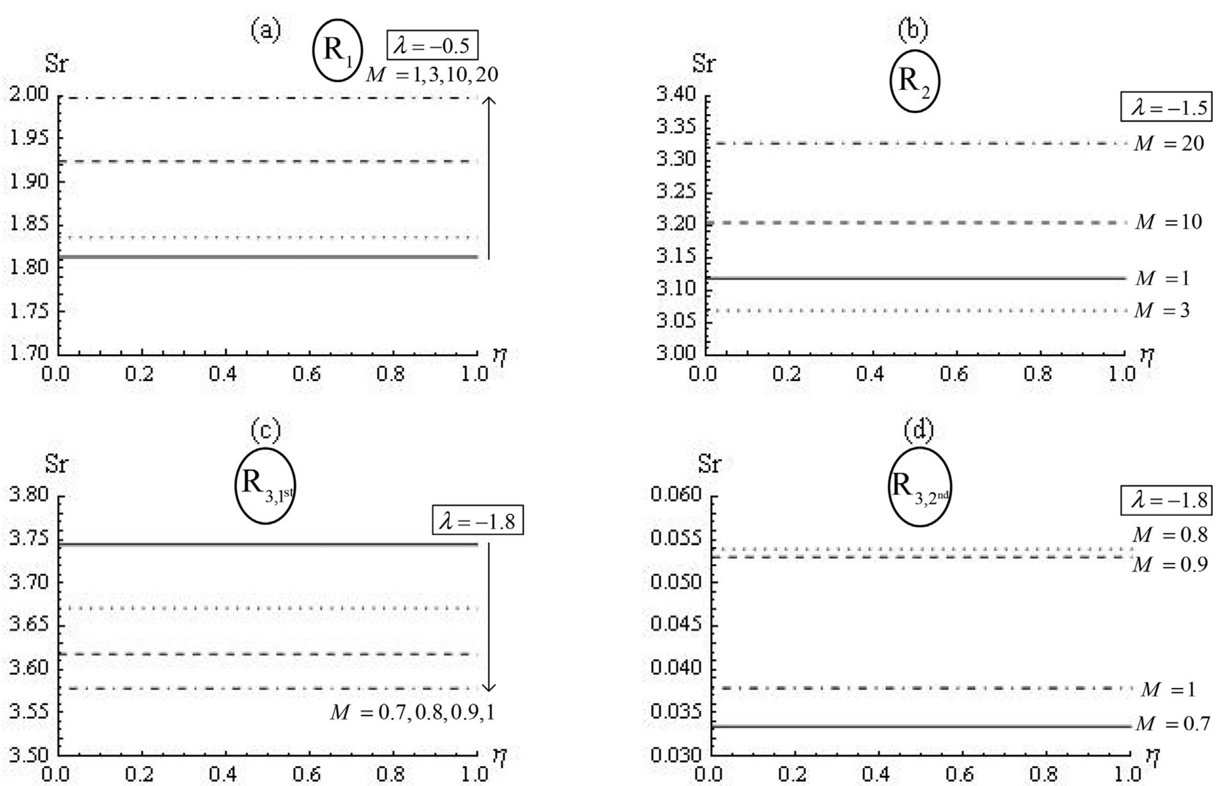

Fig. 17. Variation of the reduced skin friction coefficient (Sr) of the hybrid nanofluid Cu–Al$_2$O$_3$/H$_2$O as a function of η for various values of M, $\lambda < 0$ (shrinking sheet) and different regions; (a) R_1, (b) R_2, (c) first solution in $R_{(3,1^{st})}$ and (d) second solution in $R_{(3,2^{nd})}$, where $\delta = 1$.

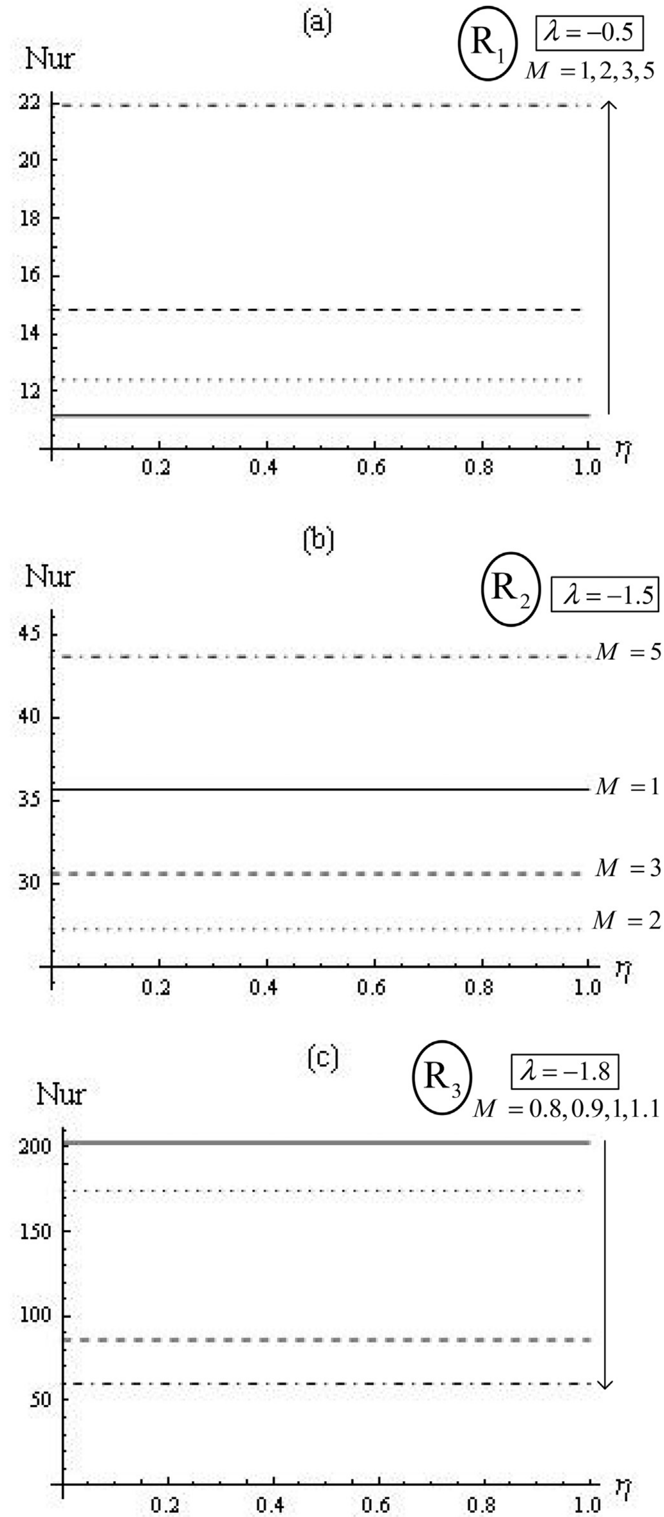

Fig. 18. Variation of the reduced Nusselt number (Nur) of the hybrid nanofluid Cu–Al_2O_3/H_2O as a function of η for various values of M, $\lambda < 0$ (shrinking sheet) and different regions, where $\delta = 1$ and $Ec = 0.1$.

where $C > 0$ for physical solutions. Now, on substituting this solution into Eq. (7) and after some manipulations, this leads to the following third order algebraic equation for C:

$$\delta \frac{\alpha_2^2}{\alpha_1} C^3 + \alpha_2 (1 - \delta\eta)\, C^2 - \left[\alpha_1 \eta + \delta \alpha_2 \left(2 + \frac{\alpha_3}{\alpha_1} M\right)\right] C - \alpha_1 (\lambda + 1) - \alpha_3 M = 0. \quad (15)$$

The three solutions of this equation, say C_1, C_2 and C_3, are theoretically given in the Appendix. It should be mentioned that the question of existence solutions to the non–linear boundary value problem (7) and (9) is converted into a question of whether the polynomial (15) has positive real roots.

4. Numerical solution for the temperature

In the spectral methods, increasing the number of degrees-of-freedom N leads to the interval h between grid points to become smaller. This causes the error to rapidly decrease even if order of the method is fixed. For example, when h increases from 10 to 20, the error becomes $O(h^{20})$ in terms of the new, smaller h. Since h is $O\left(\frac{1}{N}\right)$, we get

$$\text{Pseudospectral error} \approx O\left[\left(\frac{1}{N}\right)^N\right]. \quad (16)$$

Hence, the error is decreasing faster than any finite power of N because the power in the error formula is always increasing. This is “infinite order” or “exponential” convergence [60]. Therefore, when many decimal places of accuracy are needed, the contest between pseudospectral algorithms and finite difference is not an even battle but a rout: pseudospectral methods win hands-down. Hence, the spectral methods are preferred by engineers and mathematicians who need accurate many decimal places [60]. To decrease the roundoff error, specially on increasing N or the number of equations, Elbarbary and El-Sayed [61] have introduced a new pseudospectral differentiation matrix to decrease the roundoff error.

The resulting non–linear ordinary differential equation of $\theta(\eta)$ in Eq. (8) subject to the boundary conditions (9) is numerically solved using Chebyshev pseudospectral differentiation matrix (ChPDM), where the error becomes nearly zero ([62,63]). For implementation of ChPDM approach, it is advised to read the references [64–68]). Here, one supposes that domain of the present problem is $[0, \eta_\infty]$, where η_∞ is the edge of the boundary–layer. Therefore, the following algebraic mapping

$$\gamma = \frac{2\eta}{\eta_\infty} - 1 \quad (17)$$

transfers the domain to the Chebyshev one, i.e. $[-1, 1]$, where the associated collocation points in this interval is given by

$$\gamma_j = \cos\left(\frac{\pi}{N} j\right), \quad j = 0, 1, \ldots, N. \quad (18)$$

Then, the k^{th} derivative of any function, say $\mathbf{F}(\gamma)$, at these collocation points can be approximated by the equation:

$$\mathbf{F}^{(k)} = D^{(k)} \mathbf{F}, \quad (19)$$

where $D^{(k)}\mathbf{F}$ is the Chebyshev pseudospectral approximation of $\mathbf{F}^{(k)}$ where $\mathbf{F} = [F(\gamma_0), F(\gamma_1), \ldots, F(\gamma_N)]^T$ and $\mathbf{F}^{(k)} = [F^{(k)}(\gamma_0), F^{(k)}(\gamma_1), \ldots, F^{(k)}(\gamma_N)]^T$. The entries of the matrix $D^{(k)}$ are given by,

$$d_{i,j}^{(k)} = \frac{2\Omega_j}{N} \sum_{r=k}^{N} \sum_{\substack{\ell = 0 \\ (\ell + r - k)\, even}}^{r-k} \Omega_r\, b_{\ell,r}^{k}\, (-1)^{\left[\frac{rj + \ell i}{N}\right]} \gamma_{rj - N\left[\frac{rj}{N}\right]}\, \gamma_{ni - N\left[\frac{ni}{N}\right]}, \quad (20)$$

where $\Omega_j = 1$, except for $\Omega_0 = \Omega_N = \frac{1}{2}$ and

$$b_{\ell,r}^{k} = \frac{2^k r}{(k-1)!\, c_\ell} \frac{(\chi - \ell + k - 1)!\,(\chi + k - 1)!}{(\chi)!\,(\chi - \ell)!}, \quad (21)$$

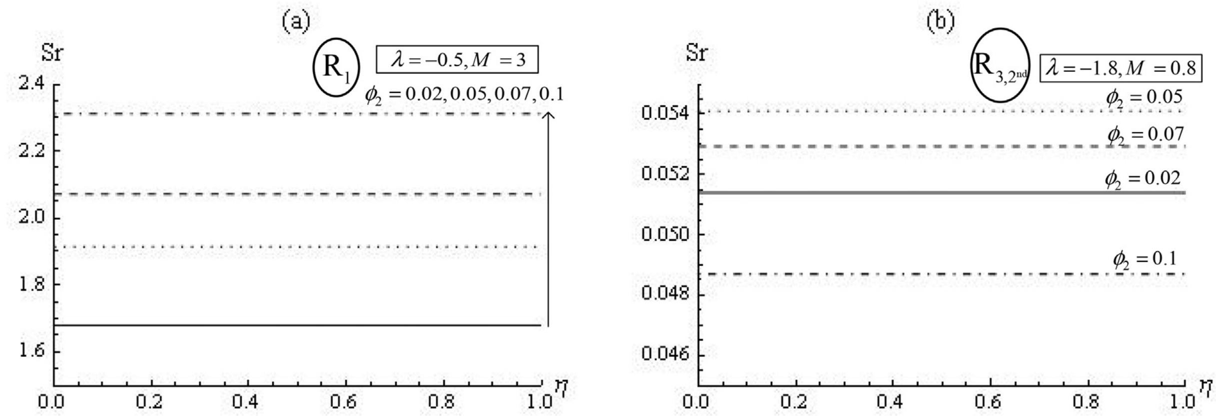

Fig. 19. Variation of the reduced skin friction coefficient (Sr) of the hybrid nanofluid Cu–Al_2O_3/H_2O as a function of η for various values of ϕ_2 where $\lambda<0$ (shrinking sheet); (a) $\lambda=-0.5$, $M=3$ (R_1) and (b) $\lambda=-1.8$, $M=0.8$ (second solution in R_3).

where $2\chi=r+\ell-k$ and $c_0=2, c_j=1, j\geq 1$. The elements $d_{0,1}^{(k)}$ are the major elements concerning its values. Therefore, on applying the ChPDM approach, derivatives of the function $\theta(\gamma)$ at the points γ_i are given by

$$\theta^{(k)}\left(\gamma_j\right)=\sum_{j=0}^{N} d_{i,j}^{(k)}\theta\left(\gamma_j\right), \quad k=1,2, \quad i=1,2,\ldots,N. \tag{22}$$

Hence, Eqs. (8) and (9) become

$$\frac{\alpha_5}{\alpha_4\, Pr}\sum_{j=0}^{N} d_{i,j}^{(2)}\,\theta\left(\gamma_j\right)+f\left(\gamma_j\right)\left(\frac{\eta_\infty}{2}\right)\sum_{j=0}^{N} d_{i,j}^{(1)}\,\theta\left(\gamma_j\right)$$
$$+\left(\frac{\eta_\infty}{2}\right)^2\left(-2f'\left(\gamma_j\right)\theta(\gamma_i)\right.$$
$$\left.+Ec\left[\frac{\alpha_2}{\alpha_1}\left(f''\left(\gamma_j\right)\right)^2+\alpha_3\left(f'\left(\gamma_j\right)-1\right)^2\right]\right)=0, \tag{23}$$

$$\theta(\gamma_N)=1, \quad \theta(\gamma_0)=0. \tag{24}$$

The resulting nonlinear Eq. (23) is associated with the boundary conditions Eqs. (24) that contain $2N$ equations for the unknowns $\theta(\gamma_j), j=1,2,\ldots,N$, which are solved using Newton method. The computer program of the numerical method was executed in MATHEMATICA 9^{TM} running on a PC.

5. Special case when $\lambda=1$

For the stretching sheet when $\lambda=1$, as seen from Eq. (14), solution of the stream function reduces to $f(\eta)=\eta$. Therefore, Eq. (8) becomes

$$\theta''(\eta)+\alpha_6\,\eta\,\theta'(\eta)-2\,\alpha_6\,\theta(\eta)=0, \tag{25}$$

which has to be solved subject to the following boundary conditions

$$\theta(0)=1, \quad \text{and} \quad \theta(\eta)\to 0 \quad \text{as} \quad \eta\to\infty, \tag{26}$$

where $\alpha_6=\dfrac{\alpha_4\, Pr}{\alpha_5}$. Now, we look for a general solution of Eq. (25), subject to the boundary conditions (26), by making the following transformations [69].

$$\theta(\eta)=Z\,e^{-\frac{\alpha_6}{4}\eta^2} \quad \text{and} \quad \eta=\frac{Y}{\sqrt{\alpha_6}}, \tag{27}$$

where Z and Y are new dependent and independent variables, respectively. Then Eq. (25) becomes

$$\frac{d^2Z}{dY^2}+\left(-3+\frac{1}{2}-\frac{Y^2}{4}\right)Z=0. \tag{28}$$

Eq. (28) is Weber equation and thus we obtain the temperature solution as;

$$\theta(\eta)=\alpha_6\,2^{-\frac{5}{4}}\,\eta^{-\frac{1}{2}}\,e^{-\frac{\alpha_6}{4}\eta^2}\,\mathrm{W}_{\left(\frac{-5}{4},\frac{-1}{4}\right)}\left(\frac{\alpha_6}{2}\eta^2\right), \tag{29}$$

where $\mathrm{W}_{(p,q)}$ is Whittaker function, see Whittaker and Watson [70].

6. Results and discussion

6.1. Studying the case of stretching sheet ($\lambda>0$)

Eq. (14) with the special case of $\lambda=1$ in Section 4 refer that the value of $\lambda \gtrless 1$ plays a very important role in analysis of the stream function and, hence, the temperature. This view is noted in Figs. 2–10 which show the velocity profiles and temperature distributions of nanofluid (Al_2O_3/H_2O) vt. hybrid nanofluid (Cu–Al_2O_3/H_2O), as applicable, in the case of stretching sheet ($\lambda>0$) for various values and different cases of the investigated parameters.

Fig. 2 indicates that, by an increase of λ when $\lambda<1$, the velocity increases until $\eta\simeq 0.8$ with $f'_{hnf}<f'_{nf}$ but $f'_{hnf}>f'_{nf}$ after this value. However, when $\lambda>1$, this behavior becomes absolutely inverse. In addition, as shown in Figs. 3 and 4, exactly the same results are obtained with the influences of M and δ on the velocity profiles. Further, effect of ϕ_2 on the hybrid nanofluid flow displays in Fig. 5 with plots (1) and (2). From this figure, it is noticed that no effect of ϕ_2 can be considered for the values of M, λ and δ in plot (1). Moreover, for the small values of M, λ and δ in plot (2) and by an increase of ϕ_2, the velocity slightly increases until $\eta\simeq 1.7$ but decreases after this value.

The temperature distribution $\theta(\eta)$ increases by increasing λ, δ and ϕ_2, with $\lambda<1$, as shown in Figs. 6, 8 and 9, respectively. However, it decreases on increasing M, ϕ_2 (with $\lambda>1$) and Ec, as indicated in Figs. 7, 9 and 10, respectively. Further, from these figures, one can see also that

$$\theta|_{Al_2O_3/H_2O}<\theta|_{Cu/H_2O}<\theta|_{Cu-Al_2O_3/H_2O}, \tag{30}$$

on studying M, i.e. the hybrid nanofluid is better as a heater rather than the both type of nanofluids. Furthermore,

$$\theta|_{Cu/H_2O}<\theta|_{Cu-Al_2O_3/H_2O}<\theta|_{Al_2O_3/H_2O}, \tag{31}$$

on investigating λ, δ and *Ec*. This means that Cu-Al_2O_3/H_2O hybrid nanofluid is better as a cooler (heater) in comparing with Al_2O_3/H_2O nanofluid (Cu/H_2O nanofluid).

6.2. Studying the case of shrinking sheet (λ < 0)

6.2.1. Critical regions of unique/dual solution

On investigating the solution's type of $f(\eta)$ and regarding Eq. (15), we suppose that

$$M_c = -\frac{\alpha_1}{\alpha_3}(\lambda+1), \quad \lambda \leq -1, \tag{32}$$

where the suffix $(\ )_c$ refers the critical value of the magnetic parameter. Therefore, on studying existence of the solution for Eq. (7) with boundary conditions in (9), we have the following two cases:

1. A unique solution is obtained when $-1 \leq \lambda < 0$ for any value of M and $\lambda < -1$ with $M \geq M_c$.
2. Dual solution is only secured when $\lambda < -1$ with $0 \leq M < M_c$.

For more details and in deeper understanding, the reader is advised to refer to the published work of Aly ([71–73]) and Aly and Pop [74]. Therefore, Fig. 11 presents the regions of unique and dual solutions of M as a function of $\lambda < 0$ (shrinking sheet) when $\delta = 1$ and $\phi_1 = 0.1$ for (a) hybrid nanofluid where $\phi_2 = 0.04$, (b) terminated line of hybrid nanofluid ($\phi_2 = 0.04$) versus nanofluid ($\phi_2 = 0$) and (c) various values of ϕ_2. In addition, in Fig. 11(a), R_i ($i = 1,2,3$) determine regions one, two and three, respectively, which are to be studied in the next section. As shown in Fig. 11(b), it is clear that region of the dual solution of the hybrid nanofluid is remarkably bigger than that of the nanofluid. In addition, dual solution region of the hybrid nanofluid exhibits little increase via increasing the nanoparticle volume fraction ϕ_2, see Fig. 11 (c). Furthermore, Table 2 indicates some values of the unique and dual solutions at different values of λ vt. M for the hybrid nanofluid. From this table, one can observe that as M increases; C_2 increases while C_3 decreases until it becomes zero when $M = M_c$, while a unique solution is only obtained for $M > M_c$.

6.2.2. Comparison of the studying parameters in the three regions

Figs. 12–15 indicate the velocity profiles and temperature distributions of the first solution for various values of M and $\lambda < 0$ (shrinking sheet) on the three regions, as shown in Fig. 11(a). Furthermore, Fig. 16 displays the influence of Eckert number on the first solution for hybrid nanofluid Cu–Al_2O_3/H_2O when $\lambda = -0.5$. The values of every parameter are introduced in the applicable figure.

Fig. 12 shows that the velocity behavior looks similar in the three regions where $f'_{hnf} < f'_{nf}$ until a specific value of η, say η_s, ($\eta_s \simeq 0.8$ in R_1, R_2 and $\eta_s \simeq 0.6$ in R_3) but $f'_{hnf} > f'_{nf}$ after this value. In addition, $f'_{R_1} < f'_{R_2} < f'_{R_3}$ in $(0,\eta_s)$, which means that the velocity reaches to the stability manner in R_1 more faster than in the other regions. This view is clearly seen in Fig. 13(a) on comparing the velocity in the three regions at the same value of the magnetic parameter; $M = 1$. However, it should be mentioned here that the velocity solutions are only available close to the terminated line in R_3, see Fig. 11. These solutions finish for combinations of M and λ away of this line as shown in Fig. 13(b). Moreover, Fig. 13 (c) exhibits that this passing away becomes dramatically on increasing the value of |λ|.

As indicated in Fig. 14, the temperature distributions are totally different over the three regions on increasing M. In particular, $\theta(\eta)$ decreases in R_1, increases–decreases in R_2 and finally increases in R_3, as shown in 14(a), 14(b) and 14(c), respectively. On comparing the temperature in the three regions for various values of λ at $M = 1$, it is found that $\theta_{R_1} > \theta_{R_2} > \theta_{R_3}$ as presented in 15(a). Further, Fig. 15 (b) secures the previous point as the temperature solutions can be

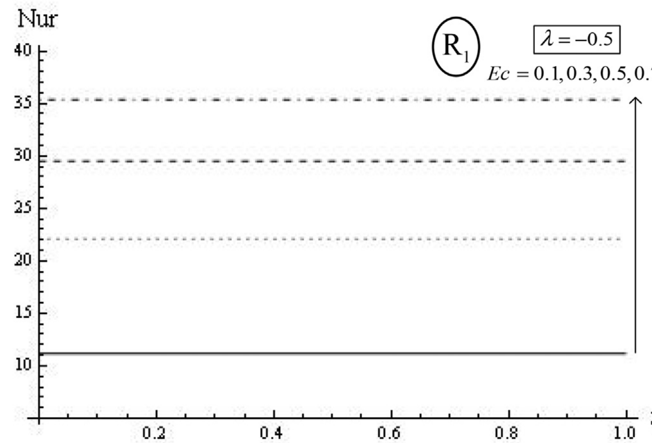

Fig. 20. Variation of the reduced Nusselt number (Nur) of the hybrid nanofluid Cu–Al_2O_3/H_2O as a function of η for various values of Ec where $\lambda = -0.5$ (shrinking sheet), $M = 1$ (R_1) and $\delta = 1$.

only obtained on choosing the values of the related physical parameters close to the terminated line in R_3, otherwise, $\theta(\eta)$ is died when $\lambda < -1.92$. This point confirms on noting that η_∞ when $\lambda = -1.92$ is tiny; about 0.04.

Influence of Eckert number (Ec) on the temperature distributions for Cu–Al_2O_3/H_2O when $\lambda = -0.5$ is plotted in Fig. 16 by taking the required values out of R_1. This figure introduces that $\theta(\eta)$ decreases on increasing Ec. It should be stated here that exactly the same behavior is also reported on investigating the effect of Ec in R_2 and R_3.

Figs. 17–20 show variation of the reduced skin friction coefficient (Sr) and reduced Nusselt number (Nur), respectively, of the hybrid nanofluid Cu–Al_2O_3/H_2O as a function of η for various values of the magnetic parameter (M), solid volume fraction (ϕ_2), Eckert number (Ec) and $\lambda < 0$ (shrinking sheet) in the three different regions. From Figs. 17 (a) and (c), one can notice that the magnetic parameter increases and decreases, respectively, by an increase of M. However, it decreases and then increases as M increases as shown in 17(b). Moreover, an inverse behavior is to be easily noticed in 17(d); i.e. Sr then decreases on increasing M. This means that, on increasing the magnetic parameter, behavior of the reduced skin friction coefficient in R_1 and R_2 are opposite to those in R_3 for the first and second solutions, respectively. Further, as seen from Figs. 18(a) and (c), Nur increases and decreases on increasing M in R_1 and R_3, respectively. Furthermore, Nur in 18(b) acts as Sr in 17 (b). Now, Figs. 19(a) and (b) show that Sr increases by increasing ϕ_2 in R_1, similar result is obtained for R_2 and $R_{(3,1^{st})}$, while in $R_{(3,2^{nd})}$ its behavior looks alike as in Fig. 17(d). Moreover, as illustrated in Fig. 20, Nur increases on increasing Ec in R_1, same as in R_2 and R_3.

7. Conclusion

In this research, the steady two–dimensional MHD boundary layer flow and heat transfer of a hybrid nanofluid over a stretching/shrinking plate with partial slip has been studied. It was assumed that the hybrid nanofluid is electrically conductive with Joule heating. Further, these investigated sheets were embedded in water-based containing nanoparticles of aluminum oxide (Al_2O_3) and then copper (Cu). In particular, Al_2O_3 in the nano–scale was initially inserted with $\phi_1 = 0.1$, which is fixed throughout the problem hereafter, to form the regular nanofluid namely Al_2O_3/H_2O. The copper was then added with various solid volume fraction (ϕ_2) to make a mixture called the hybrid nanofluid Cu–Al_2O_3/H_2O.

Upon applying the appropriate transformations, the governing equations of the problem were turned into ordinary equations which were then solved exactly and numerically for the stream function and temperature, respectively. In addition, in the special case of $\lambda = 1$ (stretching sheet), the temperature distribution was theoretically deduced as a model of Whittaker function. It was found that the hybrid nanofluid Cu–Al_2O_3/water is better as a heater on increasing the magnetic parameter. However, on increasing Eckert number, the stretching and slip parameters, it is better as a cooler (heater) in comparing with Al_2O_3/water (Cu/water).

Further, when $\lambda < 0$, unique and dual solutions exist for a certain range of the magnetic parameter. In addition, study was performed to determine the stability of the unique/dual solution, thus, it was revealed that only one of them is stable while the other is not. Furthermore, when $-1 < \lambda < 0$, the velocity reached the stability manner more faster than of $\lambda < -1$. Moreover, the velocity and temperature are only available close to the terminated line in R_3 of the dual solution. Finally, it was proved that behavior of the velocity and temperature are different over the three regions of stability.

Declaration of conpeting interest

This is to confirm that this work has not been published previously, that it is not under consideration for publication elsewhere, that its publication is approved by all authors and tacitly or explicitly by the responsible authorities where the work was carried out, and that, if accepted, it will not be published elsewhere in the same form, in English or in any other language, including electronically without the written consent of the copyright-holder.

Acknowledgement

This work was funded by the University of Jeddah, Saudi Arabia, under grant No. (UJ-02-018-DR). The authors, therefore, acknowledge with thanks the University technical and financial support.

The work of I. Pop was supported from the grant PN-III-P4-ID-PCE-2016-0036, UEFISCDI, Romania.

Appendix

$$
\begin{aligned}
C_1 = {} & \frac{-\alpha_1\alpha_2+\alpha_1\alpha_2\delta\eta}{3\alpha_2^{2^2}\delta} + \Big(2^{1/3}\Big(-3\alpha_2^2\delta(2\alpha_1\alpha_2\delta+M\alpha_2\alpha_3\delta+\alpha_1^2\eta)-(-\alpha_1\alpha_2+\alpha_1\alpha_2\delta\eta)^2\Big)\Big)\Big/ \\
& \Big(3\alpha_2^2\delta\Big(2\alpha_1^3\alpha_2^3-9\alpha_1^2\alpha_2^4\delta^2-18M\alpha_1\alpha_2^4\alpha_3\delta^2+3\alpha_1^3\alpha_2^3\delta\eta-18\alpha_1^2\alpha_2^4\delta^3\eta-9M\alpha_1\alpha_2^4\alpha_3\delta^3\eta-3\alpha_1^3\alpha_2^3\delta^2\eta^2 \\
& -2\alpha_1^3\alpha_2^3\delta^3\eta^3-27\alpha_1^2\alpha_2^4\delta^2\lambda+\surd\Big(4\Big(-3\alpha_2^2\delta(2\alpha_1\alpha_2\delta+M\alpha_2\alpha_3\delta+\alpha_1^2\eta)-(-\alpha_1\alpha_2+\alpha_1\alpha_2\delta\eta)^2\Big)^3 \\
& +(2\alpha_1^3\alpha_2^3-9\alpha_1^2\alpha_2^4\delta^2-18M\alpha_1\alpha_2^4\alpha_3\delta^2+3\alpha_1^3\alpha_2^3\delta\eta-18\alpha_1^2\alpha_2^4\delta^3\eta-9M\alpha_1\alpha_2^4\alpha_3\delta^3\eta \\
& -3\alpha_1^3\alpha_2^3\delta^2\eta^2-2\alpha_1^3\alpha_2^3\delta^3\eta^3-27\alpha_1^2\alpha_2^4\delta^2\lambda)^2\Big)\Big)^{1/3}\Big)-\frac{1}{32^{1/3}\alpha_2^2\delta} \\
& \Big(2\alpha_1^3\alpha_2^3-9\alpha_1^2\alpha_2^4\delta^2-18M\alpha_1\alpha_2^4\alpha_3\delta^2+3\alpha_1^3\alpha_2^3\delta\eta-18\alpha_1^2\alpha_2^4\delta^3\eta-9M\alpha_1\alpha_2^4\alpha_3\delta^3\eta-3\alpha_1^3\alpha_2^3\delta^2\eta^2 \\
& -2\alpha_1^3\alpha_2^3\delta^3\eta^3-27\alpha_1^2\alpha_2^4\delta^2\lambda+\surd\Big(4\Big(-3\alpha_2^2\delta(2\alpha_1\alpha_2\delta+M\alpha_2\alpha_3\delta+\alpha_1^2\eta)-(-\alpha_1\alpha_2+\alpha_1\alpha_2\delta\eta)^2\Big)^3 \\
& +(2\alpha_1^3\alpha_2^3-9\alpha_1^2\alpha_2^4\delta^2-18M\alpha_1\alpha_2^4\alpha_3\delta^2+3\alpha_1^3\alpha_2^3\delta\eta-18\alpha_1^2\alpha_2^4\delta^3\eta-9M\alpha_1\alpha_2^4\alpha_3\delta^3\eta \\
& -3\alpha_1^3\alpha_2^3\delta^2\eta^2-2\alpha_1^3\alpha_2^3\delta^3\eta^3-27\alpha_1^2\alpha_2^4\delta^2\lambda)^2\Big)\Big)^{1/3}
\end{aligned}
$$

$$
\begin{aligned}
C_2 = {} & \frac{-\alpha_1\alpha_2+\alpha_1\alpha_2\delta\eta}{3\alpha_2^2\delta} - \Big(\Big(1+i\sqrt{3}\Big)\Big(-3\alpha_2^2\delta(2\alpha_1\alpha_2\delta+M\alpha_2\alpha_3\delta+\alpha_1^2\eta)-(-\alpha_1\alpha_2+\alpha_1\alpha_2\delta\eta)^2\Big)\Big)\Big/ \\
& \Big((32^{2/3}\alpha_2^2\delta\Big(2\alpha_1^3\alpha_2^3-9\alpha_1^2\alpha_2^4\delta^2-18M\alpha_1\alpha_2^4\alpha_3\delta^2+3\alpha_1^3\alpha_2^3\delta\eta-18\alpha_1^2\alpha_2^4\delta^3\eta-9M\alpha_1\alpha_2^4\alpha_3\delta^3\eta \\
& -3\alpha_1^3\alpha_2^3\delta^2\eta^2-2\alpha_1^3\alpha_2^3\delta^3\eta^3-27\alpha_1^2\alpha_2^4\delta^2\lambda+\surd\Big(4\Big(-3\alpha_2^2\delta(2\alpha_1\alpha_2\delta+M\alpha_2\alpha_3\delta+\alpha_1^2\eta)-(-\alpha_1\alpha_2+\alpha_1\alpha_2\delta\eta)^2\Big)^3 \\
& +(2\alpha_1^3\alpha_2^3-9\alpha_1^2\alpha_2^4\delta^2-18M\alpha_1\alpha_2^4\alpha_3\delta^2+3\alpha_1^3\alpha_2^3\delta\eta-18\alpha_1^2\alpha_2^4\delta^3\eta \\
& -9M\alpha_1\alpha_2^4\alpha_3\delta^3\eta-3\alpha_1^3\alpha_2^3\delta^2\eta^2-2\alpha_1^3\alpha_2^3\delta^3\eta^3-27\alpha_1^2\alpha_2^4\delta^2\lambda)^2\Big)\Big)^{1/3}\Big)+\frac{1}{62^{1/3}\alpha_2^2\delta}\Big(1-i\sqrt{3}\Big) \\
& \Big(2\alpha_1^3\alpha_2^3-9\alpha_1^2\alpha_2^4\delta^2-18M\alpha_1\alpha_2^4\alpha_3\delta^2+3\alpha_1^3\alpha_2^3\delta\eta-18\alpha_1^2\alpha_2^4\delta^3\eta-9M\alpha_1\alpha_2^4\alpha_3\delta^3\eta-3\alpha_1^3\alpha_2^3\delta^2\eta^2 \\
& -2\alpha_1^3\alpha_2^3\delta^3\eta^3-27\alpha_1^2\alpha_2^4\delta^2\lambda+\surd\Big(4\Big(-3\alpha_2^2\delta(2\alpha_1\alpha_2\delta+M\alpha_2\alpha_3\delta+\alpha_1^2\eta)-(-\alpha_1\alpha_2+\alpha_1\alpha_2\delta\eta)^2\Big)^3 \\
& +(2\alpha_1^3\alpha_2^3-9\alpha_1^2\alpha_2^4\delta^2-18M\alpha_1\alpha_2^4\alpha_3\delta^2+3\alpha_1^3\alpha_2^3\delta\eta-18\alpha_1^2\alpha_2^4\delta^3\eta-9M\alpha_1\alpha_2^4\alpha_3\delta^3\eta \\
& -3\alpha_1^3\alpha_2^3\delta^2\eta^2-2\alpha_1^3\alpha_2^3\delta^3\eta^3-27\alpha_1^2\alpha_2^4\delta^2\lambda)^2\Big)\Big)^{1/3}
\end{aligned}
$$

$$C_3=\frac{-\alpha_1\alpha_2+\alpha_1\alpha_2\delta\eta}{3\alpha_2^2\delta}-\Big(\Big(1-i\sqrt{3}\Big)\Big(-3\alpha_2^2\delta(2\alpha_1\alpha_2\delta+M\alpha_2\alpha_3\delta+\alpha_1^2\eta)-(-\alpha_1\alpha_2+\alpha_1\alpha_2\delta\eta)^2\Big)\Big)\Big/$$

$$\Big((32^{2/3}\alpha_2^2\delta\Big(2\alpha_1^3\alpha_2^3-9\alpha_1^2\alpha_2^4\delta^2-18M\alpha_1\alpha_2^4\alpha_3\delta^2+3\alpha_1^3\alpha_2^3\delta\eta-18\alpha_1^2\alpha_2^4\delta^3\eta-9M\alpha_1\alpha_2^4\alpha_3\delta^3\eta$$

$$-3\alpha_1^3\alpha_2^3\delta^2\eta^2-2\alpha_1^3\alpha_2^3\delta^3\eta^3-27\alpha_1^2\alpha_2^4\delta^2\lambda+\surd\Big(4\Big(-3\alpha_2^2\delta(2\alpha_1\alpha_2\delta+M\alpha_2\alpha_3\delta+\alpha_1^2\eta)-(-\alpha_1\alpha_2+\alpha_1\alpha_2\delta\eta)^2\Big)^3$$

$$+(2\alpha_1^3\alpha_2^3-9\alpha_1^2\alpha_2^4\delta^2-18M\alpha_1\alpha_2^4\alpha_3\delta^2+3\alpha_1^3\alpha_2^3\delta\eta-18\alpha_1^2\alpha_2^4\delta^3\eta$$

$$-9M\alpha_1\alpha_2^4\alpha_3\delta^3\eta-3\alpha_1^3\alpha_2^3\delta^2\eta^2-2\alpha_1^3\alpha_2^3\delta^3\eta^3-27\alpha_1^2\alpha_2^4\delta^2\lambda)^2\Big)\Big)^{1/3}\Big)+\frac{1}{62^{1/3}\alpha_2^2\delta}\Big(1+i\sqrt{3}\Big)$$

$$\Big(2\alpha_1^3\alpha_2^3-9\alpha_1^2\alpha_2^4\delta^2-18M\alpha_1\alpha_2^4\alpha_3\delta^2+3\alpha_1^3\alpha_2^3\delta\eta-18\alpha_1^2\alpha_2^4\delta^3\eta-9M\alpha_1\alpha_2^4\alpha_3\delta^3\eta-3\alpha_1^3\alpha_2^3\delta^2\eta^2$$

$$-2\alpha_1^3\alpha_2^3\delta^3\eta^3-27\alpha_1^2\alpha_2^4\delta^2\lambda+\surd\Big(4\Big(-3\alpha_2^2\delta(2\alpha_1\alpha_2\delta+M\alpha_2\alpha_3\delta+\alpha_1^2\eta)-(-\alpha_1\alpha_2+\alpha_1\alpha_2\delta\eta)^2\Big)^3$$

$$+(2\alpha_1^3\alpha_2^3-9\alpha_1^2\alpha_2^4\delta^2-18M\alpha_1\alpha_2^4\alpha_3\delta^2+3\alpha_1^3\alpha_2^3\delta\eta-18\alpha_1^2\alpha_2^4\delta^3\eta-9M\alpha_1\alpha_2^4\alpha_3\delta^3\eta$$

$$-3\alpha_1^3\alpha_2^3\delta^2\eta^2-2\alpha_1^3\alpha_2^3\delta^3\eta^3-27\alpha_1^2\alpha_2^4\delta^2\lambda)^2\Big)\Big)^{1/3}$$

References

[1] S.U.S. Choi, Enhancing thermal conductivity of fluids with nanoparticles, Proceedings of the 1995 ASME International Mechanical Engineering Congress and Exposition, FED 231/MD 66 1995, pp. 99–105.

[2] K.S. Hwang, J.H. Lee, S.P. Jang, Buoyancy–driven heat transfer of water–based Al_2O_3 nanofluids in a rectangular cavity, Int. J. Heat Mass Transf. 50 (2007) 4003–4010.

[3] Y. Wang, G.H. Su, Experimental investigation on nanofluid flow boiling heat transfer in a vertical tube under different pressure conditions, Exp. Thermal Fluid Sci. 77 (2016) 116–123.

[4] M. Ahmadi, G. Willing, Heat transfer measurement in water based nanofluids, Int. J. Heat Mass Transf. 118 (2018) 40–47.

[5] J. Buongiorno, Convective transport in nanofluids, ASME J. Heat Transfer 128 (2006) 240–250.

[6] R.K. Tiwari, M.K. Das, Heat transfer augmentation in a two–sided lid–driven differentially heated square cavity utilizing nanofluids, Int. J. Heat Mass Transf. 50 (2007) 2002–2018.

[7] A.V. Kuznetsov, D.A. Nield, Natural convective boundary–layer flow of a nanofluid past a vertical plate, Int. J. Therm. Sci. 49 (2010) 243–247.

[8] A.M. Rohni, S. Ahmad, I. Pop, Boundary layer flow over a moving surface in a nanofluid beneath a uniform free stream, Int. J. Heat Fluid Flow 21 (2011) 828–846.

[9] N. Bachok, A. Ishak, I. Pop, Flow and heat transfer over a rotating porous disk in a nanofluid, Phys. B Condens. Matter 406 (2011) 1767–1772.

[10] A.M. Rohni, S. Ahmad, I. Pop, Flow and heat transfer over an unsteady shrinking sheet with suction in nanofluids, Int. J. Heat Mass Transf. 55 (2012) 1888–1895.

[11] A.J. Chamkha, M. Molana, A. Rahnama, F. Ghadami, On the nanofluids applications in microchannels: A comprehensive review, Powder Technol. 332 (2018) 287–322.

[12] A.A. Nadooshan, H. Eshgarf, M. Afrand, Evaluating the effects of different parameters on rheological behavior of nanofluids: A comprehensive review, Powder Technol. 338 (2018) 342–353.

[13] N. Sezer, M.A. Atieh, M. Koç, A comprehensive review on synthesis, stability, thermophysical properties, and characterization of nanofluids, Powder Technol. 344 (2019) 404–431.

[14] T. Ambreen, A. Saleem, H.M. Ali, S.A. Shehzad, C.W. Park, Performance analysis of hybrid nanofluid in a heat sink equipped with sharp and streamlined micro pin-fins, Powder Technol. 355 (2019) 552–563.

[15] V. Kumar, J. Sarkar, Numerical and experimental investigations on heat transfer and pressure drop characteristics of Al_2O_3–TiO_2 hybrid nanofluid in minichannel heat sink with different mixture ratio, Powder Technol. 345 (2019) 717–727.

[16] S. Suresh, K.P. Venkitaraj, P. Selvakumar, M. Chandrasekar, Effect of Al_2O_3–cu/water hybrid nanofluid in heat transfer, Exp. Thermal Fluid Sci. 38 (2012) 54–60.

[17] M. Baghbanzadeha, A. Rashidib, D. Rashtchiana, R. Lotfib, A. Amrollahib, Synthesis of spherical silica/multi wall carbon nanotubes hybrid nano structures and investigation of thermal conductivity of related nanofluids, Thermochim. Acta 549 (2012) 87–94.

[18] M. Vafaei, M. Afrand, N. Sina, R. Kalbasi, F. Sourani, H. Teimouri, Evaluation of thermal conductivity of MgO–MWCNTs/EG hybrid nanofluids based on experimental data by selecting optimal artificial neural networks, Phys. E. 85 (2017) 90–96.

[19] R. Nasrin, M.A. Alim, Finite element simulation of forced convection in a flat plate solar collector: influence of nanofluid with double nanoparticles, J. Appl. Fluid Mech. 7 (2014) 543–556.

[20] B. Takabi, H. Shokouhmand, Effects of Al_2O_3–Cu/water hybrid nanofluid on heat transfer and flow characteristics in turbulent regime, Int. J. Mod. Phys. C 26 (2015) 1550047.

[21] S.S.U. Devi, S.P.A. Devi, Numerical investigation of three-dimensional hybrid Cu–Al_2O_3/water nanofluid flow over a stretching sheet with effecting Lorentz force subject to Newtonian heating, Can. J. Phys. 94 (2016) 490–496.

[22] S.S.U. Devi, S.P.A. Devi, Heat transfer enhancement of Cu–Al_2O_3/water hybrid nanofluid flow over a stretching sheet, J. Nigerian Math. Soc. 36 (2017) 419–433.

[23] R.M. Yousefi, S. Dinarvand, M.E. Yazdi, I. Pop, Stagnation–point flow of an aqueous titania-copper hybrid nanofluid toward a wavy cylinder, Int. J. Numer. Meth. Heat Fluid Flow 28 (2018) 1716–1735.

[24] T. Hayat, S. Nadeem, A.U. Khan, Rotating flow of Ag–CuO/H_2O hybrid nanofluid with radiation and partial slip boundary effects, Euro. Phys. J. E 41 (2018) 75.

[25] S.S. Ghadikolaei, M. Yassari, H. Sadeghi, K. Hosseinzadeh, D.D. Ganji, Investigation on thermophysical properties of TiO_2-Cu/H_2O hybrid nanofluid transport dependent on shape factor in MHD stagnation point flow, Powder Technol. 322 (2017) 428–438.

[26] T. Tayebi, A.J. Chamkha, Buoyancy–driven heat transfer enhancement in a sinusoidally heated enclosure utilizing hybrid nanofluid, Comput. Thermal Sci.: An Int. J. 9 (2017) 405–421.

[27] M. Ghalambaz, M.A. Sheremet, S.A.M. Mehryan, F.M. Kashkooli, I. Pop, Local thermal non–equilibrium analysis of conjugate free convection within a porous enclosure occupied with Ag–MgO hybrid nanofluid, J. Therm. Anal. Calorimetry 135 (2019) 1381–1398.

[28] W.J. Minkowycz, E.M. Sparrow, J.P. Abraham (Eds.), Nanoparticle Heat Transfer and Fluid Flow, CRC Press, Taylor & Fracis Group, New York, 2013.

[29] A. Shenoy, M. Sheremet, I. Pop, Convective Flow and Heat Transfer from Wavy Surfaces: Viscous Fluids, Porous Media and Nanofluids, CRC Press, New York, 2016.

[30] J. Buongiorno, et al., A benchmark study on the thermal conductivity of nanofluids, J. Appl. Phys. 106 (2009) 1–14.

[31] M. Bahiraei, S. Heshmatian, H. Moayedi, Artificial intelligence in the field of nanofluids: A review on applications and potential future directions, Powder Technol. 353 (2019) 276–301.

[32] O. Mahian, L. Kolsi, M. Amani, P. Estelle, G. Ahmadi, C. Kleinstreuer, J.S. Marshalli, M. Siavashi, R.A. Taylor, H. Niazmand, S. Wongwises, T. Hayat, A. Kolanjiyil, A. Kasaeian, I. Pop, Recent advances in modeling and simulation of nanofluid flows – Part I: fundamentals and theory, Phys. Rep. 790 (2019) 1–48.

[33] O. Mahian, L. Kolsi, M. Amani, P. Estelle, G. Ahmadi, C. Kleinstreuer, J.S. Marshalli, M. Siavashi, R.A. Taylor, H. Niazmand, S. Wongwises, T. Hayat, A. Kolanjiyil, A. Kasaeian, I. Pop, Recent advances in modeling and simulation of nanofluid flows – Part II: applications, Phys. Rep. 791 (2019) 1–59.

[34] J. Sarkarn, P. Ghosh, A. Adil, A review on hybrid nanofluids: recent research, development and applications, Renew. Sust. Energ. Rev. 43 (2015) 164–177.

[35] J.R. Babu, K.K. Kumar, S.S. Rao, State-of-art review on hybrid nanofluids, Renew. Sust. Energ. Rev. 77 (2017) 551–565.

[36] G. Huminic, A. Huminic, Heat transfer capability of the hybrid nanofluids for heat transfer applications, J. Mol. Liq. 272 (2018) 857–870.

[37] N.A.C. Sidik, I.M. Adamu, M.M. Jamil, G.H.R. Kefayati, R. Mamat, G. Najafi, Recent progress on hybrid nanofluids in heat transfer applications: A comprehensive review, Int. Commun. Heat Mass Transfer 78 (2016) 68–79.

[38] L.S. Sundar, K.V. Sharma, M.K. Singh, A.C.M. Sousa, Hybrid nanofluids preparation, thermal properties, heat transfer and friction factor – a review, Renew. Sust. Energ. Rev. 68 (2017) 185–198.

[39] A. Asadi, S. Aberoumand, A. Moradikazerouni, F. Pourfattah, G. Żyla, P. Estellé, O. Mahian, S. Wongwises, H.M. Nguyen, A. Arabkoohsar, Recent advances in preparation methods and thermophysical properties of oil–based nanofluids: a state-of-the-art review, Powder Technol. 352 (2019) 209–226.
[40] Z. Aparna, M. Michael, S.K. Pabi, S. Ghosh, Thermal conductivity of aqueous Al_2O_3/Ag hybrid nanofluid at different temperatures and volume concentrations: an experimental investigation and development of new correlation function, Powder Technol. 343 (2019) 714–722.
[41] O. Gulzar, A. Qayoum, R. Gupta, Experimental study on stability and rheological behaviour of hybrid Al_2O_3-TiO_2 Therminol-55 nanofluids for concentrating solar collectors, Powder Technol. 352 (2019) 436–444.
[42] B.C. Sakiadis, Boundary–layer behaviour on continuous solid surfaces: I. Boundary layer equations for two–dimensional and axisymmetric flow, American Inst. Chem. Engineers J. 7 (1961) 26–28.
[43] L.J. Crane, Flow past a stretching plate, Z. Angew. Math. Phys. 21 (1970) 645–647.
[44] E. Magyari, B. Keller, Exact solutions for self–similar boundary-layer flows induced by permeable stretching walls, Euro. J. Mech. B/Fluids 19 (2000) 109–122.
[45] A. Ishak, R. Nazar, I. Pop, Boundary layer flow and heat transfer over an unsteady stretching vertical surface, Meccanica 44 (2009) 369–375.
[46] S. Goldstein, On backward boundary layers and flow in converging passage, J. Fluid Mech. 21 (1965) 33–45.
[47] C.Y. Wang, Liquid film on an unsteady stretching sheet, Q. Appl. Math. 48 (1990) 601–610.
[48] M. Miklavčič, C.Y. Wang, Viscous flow due to a shrinking sheet, Q. Appl. Math. 64 (2006) 283–290.
[49] T. Fang, J. Zhang, Thermal boundary layers over a shrinking sheet: an analytical solution, Acta Mech. 209 (2010) 325–343.
[50] J.H. Merkin, V. Kumaran, The unsteady MHD boundary–layer flow on a shrinking sheet, Euro. J. Mech. B/Fluids 29 (2010) 357–363.
[51] S.K. Soid, A. Ishak, I. Pop, Unsteady MHD flow and heat transfer over a shrinking sheet with ohmic heating, Chin. J. Phys. 55 (2017) 1626–1636.
[52] I. Pop, K. Naganthran, R. Nazar, A. Ishak, The effect of vertical throughflow on the boundary layer flow of a nanofluid past a stretching/shrinking sheet: A revised model, Int. J. Numer. Meth. Heat Fluid Flow 27 (2017) 1910–1927.
[53] I. Waini, A.M. Ishak, I. Pop, Unsteady flow and heat transfer past a stretching/shrinking sheet in a hybrid nanofluid, Int. J. Heat Mass Transf. 136 (2019) 288–297.
[54] N.S. Khashi'ie, N. Md. Arifin, R. Nazar, E.H. Hafidzuddin, N. Wahi, I. Pop, Magnetohydrodynamics (MHD) axisymmetric flow and heat transfer of a hybrid nanofluid past a radially permeable stretching/shrinking sheet with Joule heating, Chin. J. Phys. 64 (2020) 251–263.
[55] I. Pop, A. Ishak, F. Aman, Radiation effects on the MHD flow near the stagnation point of a stretching sheet: revisited, J. Appl. Math. Phys. (ZAMP) 62 (2011) 953–956.
[56] S. Sheikholeslami, M. Gorji-Bandpy, D.D. Ganji, MHD free convection in an eccentric semi–annulus filled with nanofluid, J. Taiwan Inst. Chem. Eng. 45 (2014) 1204–1216.
[57] T.R. Mohapatra, A.S. Gupta, Heat transfer in stagnation–point flow towards a stretching sheet, Heat Mass Transf. 38 (2002) 517–521.
[58] T. Fang, S. Yao, Ji Zhang, A. Aziz, Viscous flow over a shrinking sheet with a second order slip flow model, Commun. Nonlinear Sci. Numer. Simul. 15 (2010) 1831–1842.
[59] R.S.R. Gorla, S. Siddiqa, M.A. Mansour, A.M. Rashad, T. Salah, Heat source/sink effects on a hybrid nanofluid–filled porous cavity, J. Thermophys. Heat Transf. 31 (2017) 847–857.
[60] J.P. Boyd, Chebyshev and Fourier Spectral Methods, Dover, New York, 2000.
[61] E.M.E. Elbarbary, S.M. El-Sayed, Higher order pseudospectral differentiation matrices, Appl. Numer. Math. 55 (2005) 425–438.
[62] E.M.E. Elbarbary, Chebyshev finite difference method for the solution of boundary–layer equations, Appl. Math. Comput. 160 (2005) 487–498.
[63] E.M.E. Elbarbary, M. El-Kady, Chebyshev finite difference approximation for the boundary value problems, Appl. Math. Comput. 139 (2003) 513–523.
[64] E.H. Aly, M. Benlahsen, M. Guedda, Similarity solutions of a MHD boundary-layer flow past a continuous moving surface, Int. J. Eng. Sci. 45 (2007) 486–503.
[65] M. Guedda, E.H. Aly, A. Ouahsine, Analytical and ChPDM analysis of MHD mixed convection over a vertical flat plate embedded in a porous medium filled with water at 4°C, Appl. Math. Model. 35 (2011) 5182–5197.
[66] E.H. Aly, K. Vajravelu, Exact and numerical solutions of MHD nano boundary–layer flows over stretching surfaces in a porous medium, Appl. Math. Comput. 232 (2014) 191–204.
[67] E.H. Aly, Radiation and MHD boundary layer stagnation-point of nanofluid flow towards a stretching sheet embedded in a porous medium: analysis of suction/injection and heat generation/absorption with effect of the slip model, Math. Probl. Eng., in the Special Issue: Macroscopic/Mesoscopic Computational Materials Science Modeling and Engineering, Vol. 2015, 2015, Article ID 563547, 20 pages.
[68] E.H. Aly, H.M. Sayed, Magnetohydrodynamic and thermal radiation effects on the boundary-layer flow due to a moving extensible surface with the velocity slip model: A comparative study of four nanofluids, J. Magn. Magn. Mater. 422 (2017) 440–451.
[69] E.H. Aly, L. Elliott, D.B. Ingham, Mixed convection boundary–layer flow over a vertical surface embedded in a porous medium, Euro. J. Mech. B/Fluids 22 (2003) 529–543.
[70] E.T. Whittaker, G.N. Watson, A Course of Modern Analysis, Cambridge, 4th ed., 1962.
[71] E.H. Aly, Existence of the multiple exact solutions for nanofluid flow over a stretching/shrinking sheet embedded in a porous medium at the presence of magnetic field with electrical conductivity and thermal radiation effects, Powder Technol. 301 (2016) 760–781.
[72] E.H. Aly, Catalogue of existence of the multiple physical solutions of hydromagnetic flow over a stretching/shrinking sheet for viscoelastic second-grade and Walter's B fluids, Phys. Scr. 94 (2019) 105223(16pp).
[73] E.H. Aly, Dual exact solutions of graphene–water nanofluid flow over stretching/shrinking sheet with suction/injection and heat source/sink: critical values and regions with stability, Powder Technol. 342 (2019) 528–544.
[74] E.H. Aly, I. Pop, MHD flow and heat transfer over a permeable stretching/shrinking sheet in a hybrid nanofluid with a convective boundary condition, Int. J. Numer. Meth. Heat Fluid Flow 29 (2019) 3012–3038.